



1 **Subtropical gyre persistence in the Gulf of Cadiz, southern Iberian margin, interrupted**
2 **by extremely cold surface water incursions during the Early – Middle Pleistocene**
3 **Transition**

4
5 Aline Mega^{1,2} (0000-0002-9386-2261), Teresa Rodrigues^{1,2} (0000-0001-7811-7506), Emília
6 Salgueiro^{1,2} (0000-0003-1000-2977), Mária Padilha¹ (0000-0002-7103-5695), Henning
7 Kuhnert³ (0000-0001-5242-4495), Antje H. L. Voelker^{1,2} (0000-0001-6465-6023)

8
9 ¹Divisão de Geologia e Georecursos Marinhos, Instituto Português do Mar e da Atmosfera
10 (IPMA), Avenida Doutor Alfredo Magalhães Ramalho 6, 1495-165 Alges, Portugal.

11 ²CCMAR Associated Laboratory, University of the Algarve, Campus de Gambelas, 8005-139
12 Faro, Portugal.

13 ³MARUM, Universität Bremen, Leobener Straße 8, 28359 Bremen, Germany.

14 *Correspondence to:* Aline Mega (alinemega20@gmail.com)

15
16 **Abstract.** Besides the shift in dominant orbital cyclicity, the mid-Pleistocene Transition or
17 Early-Middle Pleistocene Transition (EMPT) was characterized by a change in the deep
18 thermohaline circulation. Those changes contributed to more intense and longer-lasting glacial
19 periods and cooler sea surface temperatures (SSTs). Within the Atlantic Ocean, the Iberian
20 margin is considered a key location to study climatic variations influenced by both high- and
21 low-latitude processes. In this study we focus on IODP Site U1387 on the southern Portuguese
22 margin to reconstruct surface water circulation and related plankton foraminifera ecosystem
23 changes during the interval of Marine Isotope Stage (MIS) 28 to MIS 18 (1006-750 ka). Our
24 planktonic foraminifera assemblages and SST reconstructions (foraminifera assemblages and
25 $U^{K'}_{37}$ alkenone index) demonstrate warm, stable SST conditions during much of the interval
26 due to persistent influence of subtropical gyre waters as indicated by the tropical-subtropical
27 and Azores Current related foraminifera species and the periods with dominant sinistral coiling
28 direction of the species *Globorotalia truncatulinoides*. Maximum interglacial SSTs were up to
29 2°C warmer than at present in both summer and winter, with the exception of interglacial MIS
30 23 with SSTs ~1.5°C colder than in the other interglacials. Subsequent the respective glacial
31 inception, the relative warm conditions were periodically interrupted by millennial-scale
32 extreme cold events when polar species *Neogloboquadrina pachyderma* became abundant



33 (>30%) and the SSTs, reconstructed from the foraminifera assemblage data, dropped below
34 10°C in summer and 5 °C in winter. The most pronounced event, considering the amplitude of
35 cooling and duration, occurred between 870 to 864 ka, marking the terminal stadial event of
36 the MIS 22/MIS 21 transition (Termination X). Extreme cold events, always associated with
37 the incursion of subpolar waters into the Gulf of Cadiz, mark all the terminal stadial events
38 from Terminations XII to IX and the millennial-scale variability during the transitions to full
39 glacial conditions, although the duration of the cooling varied greatly. The extreme cooling
40 was only possible through migration of the subarctic front into the lower mid-latitudes as a
41 consequence of an extreme reduction in the Atlantic meridional overturning circulation. The
42 amplitude of cooling, duration, and frequency of subpolar water incursions during MIS 24 to
43 MIS 22 stands out, providing further evidence for the "900 ka event" being a key feature of the
44 EMPT.

45

46 **1. Introduction**

47 A major global climatic shift, known as the mid-Pleistocene or Early-Middle
48 Pleistocene Transition (EMPT), took place between 1250 and 650 thousand years (ka) ago,
49 dramatically changing Earth's climate dynamics (Clark, 2012; Clark et al., 2006; Head and
50 Gibbard, 2015; McClymont et al., 2013). This period was characterized by long-term cooling
51 in global mean sea surface temperatures (SSTs), lower glacial atmospheric carbon dioxide
52 levels and a change in the deep-water circulation, stratification and carbon storage during the
53 glacial periods that ultimately resulted in more intense and longer-lasting glacial periods
54 (changing from 41 kyr to 100 kyr cycles) and cooler SSTs (Chalk et al., 2017; Clark et al.,
55 2024; Farmer et al., 2019; Kim et al., 2021; Tachikawa et al., 2021; Willeit et al., 2019;
56 McClymont et al., 2013). The major shift in the deep-water circulation during the EMPT, often
57 considered as the first 100 ka cycle, is referred to as "the 900 ka event" (Farmer et al., 2019;
58 McClymont et al., 2013; Pena and Goldstein, 2014).

59 The causes of these long-term patterns of Quaternary climate have been attributed to
60 internal changes in climate response to orbital forcing, as the latter did not change over this
61 time (Clark, 2012; Clark et al., 2006; Hodell and Channell, 2016; Shackleton, 2000). It is
62 believed that the EMPT may have been influenced by ocean-atmosphere system changes, with
63 declining atmospheric carbon dioxide concentrations and continental ice-sheet growth playing
64 a role (Chalk et al., 2017; Willeit et al., 2019). During the EMPT glacials, lower sea-levels
65 contribute to benthic $\delta^{13}\text{C}$ values reaching their lowest levels in 5 million years (Westerhold et
66 al., 2020), which may be caused by exposed continental shelves accelerating the transport of



67 organic carbon into the oceans (Head and Gibbard, 2015). Nowadays, water masses carrying
68 lower $\delta^{13}\text{C}$ signals ($<0.5\text{ ‰}$) are formed by convection around Antarctica (Antarctic
69 Intermediate Water, Antarctic Bottom Water/AABW) and spread out into the global ocean
70 basins (Curry and Oppo, 2005; Kroopnick, 1985). Northward and upward expansion of such
71 signals in the Atlantic basin during glacial periods was therefore interpreted to reflect the
72 replacement of North Atlantic Deep Water (NADW) by southern sourced waters and thus a
73 reduced Atlantic Meridional Overturning Circulation (AMOC) (Hodell and Channell, 2016;
74 Raymo et al., 2004; Raymo et al., 1990; Sarnthein et al., 1994). Weakening NADW influence
75 throughout the MIS 22-MIS 24 interval is supported by neodymium isotope records (Farmer
76 et al., 2019; Kim et al., 2021; Pena and Goldstein, 2014; Tachikawa et al., 2021). A possible
77 explanation for the increase in glacial $\delta^{18}\text{O}$ values during the “900 ka event” relates a weak
78 AMOC and low insolation in the Southern Hemisphere during Marine Isotope Stage (MIS) 23
79 to maximum continental ice volume build-up, which continued to be registered in the
80 subsequent glacials (Elderfield et al., 2012; Pena and Goldstein, 2014).

81 Most of the water stored during Quaternary glaciations in the Laurentide, Greenland
82 and European ice sheets was discharged into the North Atlantic Ocean during the last 1.5 Ma,
83 producing short cold events that were often associated with ice-rafted debris (IRD) deposition
84 (Barker et al., 2022; Barker et al., 2021; Hodell and Channell, 2016; Jansen et al., 2000). The
85 effect of ice-cover changes during the EMPT, mainly associated with the “900 ka event”, has
86 been reported based on different proxies and in the (sub)polar regions of both hemispheres. In
87 the North Atlantic, Wright and Flower (2002) found extremely cold events from 1000 to 500
88 ka at ODP Sites 980 (55°N, 15°W) and 984 (61°N, 24°W) (Fig. 1), based on the percentage of
89 polar species *Neogloboquadrina pachyderma* and IRD records, later on corroborated by the
90 1.7 Ma long records for Site 983 (60°N 24°W) (Barker et al., 2011; Barker et al., 2022). These
91 data, in conjunction with increased reworked nannofossil abundance during the IRD events at
92 Sites 980/981 (Marino et al., 2011), suggest that the Arctic front shifted from a position
93 between those Sites southward and the sea-ice cover expanded greatly during those periods as
94 a result of reduced NADW production. That scenario is supported by evidence from IODP Site
95 U1314 (56.36°N, 27.88°W), where Hernández-Almeida et al. (2013) observed an abundance
96 of *N. pachyderma* of up to 93 % during the “900 ka event”. Between 900 and 675 ka, the same,
97 short-term extreme cold events were registered further south at IODP Site U1385 (Iberian
98 Margin) as cold SST events associated with lower salinities (higher percentages of the C37:4
99 alkenone) (Rodrigues et al., 2017). All those cold events were associated with a northward and
100 upward penetration of AABW and thus reduction in the AMOC depth (Hodell and Channell,



101 2016; Hodell et al., 2023a; Hernández-Almeida et al., 2015), especially during the terminal
102 stadial events.

103 The western Iberian margin is a key area for high-resolution paleoclimatic studies
104 because it is climatologically sensitive to high and low latitude processes. Following the
105 seminal work of Shackleton et al. (2000), it is known that benthic foraminifera $\delta^{18}\text{O}$ records
106 from depths greater than 2500 m on the southwestern Portuguese margin reflect an Antarctic
107 climate signal, in particular Antarctic temperature variations, whereas surface water records
108 from the western and southern Portuguese margin mimic the millennial-scale Greenland
109 interstadial/stadial oscillation and thus record northern hemisphere temperature variations. This
110 concept has now been proven for the last 1440 ka with the high-resolution records of IODP
111 Site U1385 (Hodell et al., 2023a).

112 Furthermore, planktonic foraminifera assemblages are reliable sources for
113 environmental conditions in the western Iberian margin and specific assemblages can identify
114 prevailing oceanographic conditions. At modern conditions, subtropical species, among them
115 *Globigerinoides ruber* white, reflect the influence of the Azores Current (AzC), whereas
116 *Globigerina inflata* and *Neogloboquadrina incompta* represent the Portugal Current and
117 *Globigerinoides bulloides* upwelling events (Salgueiro et al., 2008). Increased abundances of
118 *Turborotalita quinqueloba* and *Neogloboquadrina pachyderma*, on the other hand, can provide
119 insights into past incursions of subpolar waters and southward displacement of the subarctic
120 front (boundary between the subtropical and subpolar gyres) (Eynaud et al., 2009; Girone et
121 al., 2023; Johannessen et al., 1994; Martin-Garcia et al., 2015; Pflaumann et al., 2003;
122 Salgueiro et al., 2010; Singh et al., 2023).

123 Recent studies (Bajo et al., 2020a; Voelker et al., 2015) confirmed extremely cold SST
124 conditions during stadial climate events of the EMPT also at southern Portuguese margin IODP
125 Site U1387 (Fig. 1). However, detailed information on the surface-water conditions during the
126 “900 ka event” (MIS 24 to MIS 22) and during the lead up to it remains limited. This study,
127 therefore, aims to characterize surface-water conditions at IODP Site U1387 between MIS 28
128 and MIS 18 (1006-750 ka) to better understand the climate dynamics and oceanographic
129 changes that occurred during this critical period. Situated in the northern Gulf of Cadiz, Site
130 U1387 is highly sensitive to changes in the North Atlantic subtropical gyre and to the water
131 mass exchange between the North Atlantic and the Mediterranean Sea. Moreover, the high
132 sedimentation rates ($\geq 20 \text{ cm kyr}^{-1}$) in contourite drifts like the Faro drift, into which Site U1387
133 was drilled, provide exceptional paleoclimate records with high temporal resolution
134 (Hernández-Molina et al., 2016b). For evaluating temperature changes, both in terms of



135 amplitude and timing, and their relationship to the prevailing oceanographic conditions, we
136 produced high-resolution, sub-millennial-scale records of planktonic foraminifera assemblages
137 and SST reconstructions. Using a multi-proxy approach, the SSTs were reconstructed in two
138 ways: 1) converting the planktonic foraminifera assemblages into summer and winter SSTs
139 using a transfer function; and 2) based on the U^{K}_{37} alkenone index, approximately reflecting
140 annual mean SSTs. Strength in subtropical gyre circulation was inferred from the dominant
141 coiling direction of the planktonic foraminifera species *Globorotalia truncatulinoides* (Billups
142 et al., 2016). We compare our data with other available records from the southwestern Iberian
143 margin, as well as sites from the mid-latitude North Atlantic. This comparison allows us to
144 contextualize our results within broader regional and global climatic trends, providing insights
145 into the variability and connections between these key areas during the study period. By
146 integrating these records, we aim to improve our understanding of both local and large-scale
147 processes affecting this Northeast Atlantic region.

148

149 **2. Regional Setting**

150 The subtropical gyre nowadays comprises much of the surface and sub-surface waters
151 in the low-to mid-latitude North Atlantic, is approximately 1000 km in diameter and
152 distributes heat and moisture to the north (Fig. 1A). The gyre circulation is driven by a
153 combination of trade winds, westerlies and the Coriolis force, whereby the westerlies dominate
154 the circulation in its northern part, especially during the winter. The strength and position of
155 the oceanic currents depend, therefore, on the variability of the atmospheric wind fields. During
156 the winter the latter are characterized by the eastward displacement of cyclonic perturbations
157 (Relvas et al., 2007).

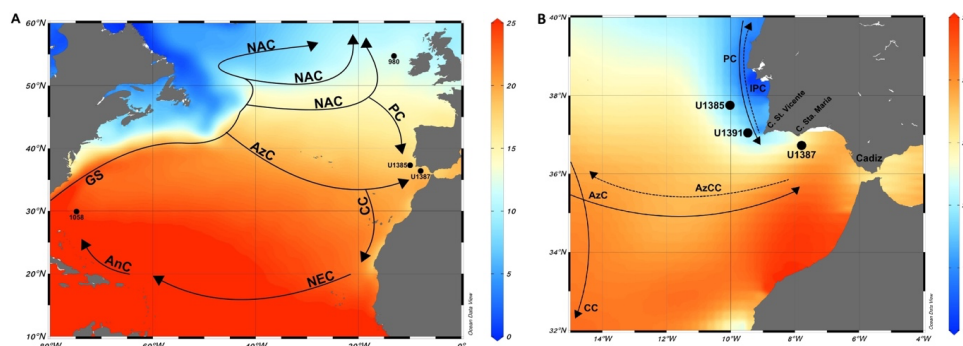
158 Located within the southern mid-latitude North Atlantic, the Gulf of Cadiz has a
159 surface-subsurface current system dominated by three branches of the North Atlantic's
160 subtropical gyre circulation: the eastward flowing AzC between 34.3 and 35.7°N, contributing
161 with heat and salt; the Azores Counter-Current between 37.74 and 39.24°N and the Canary
162 Current that flows south-westwards (Carracedo Segade et al., 2015). The AzC dominates the
163 Gulf of Cadiz surface waters (0 to 500 m) and partially recirculates along the western Iberian
164 margin through the Iberian Poleward Current that results from the seasonal reversal of the wind
165 regimes (Frouin et al., 1990; Peliz et al., 2005) (Fig. 1B). Also, the Gulf of Cadiz is an important
166 transition zone where the Mediterranean Outflow Water flows at intermediate depth level,
167 adding high salinity and heat to the North Atlantic Circulation (Ambar et al., 1999; Folkard et
168 al., 1997).



169 The Gulf of Cadiz receives contributions from the Portugal Current and the Portugal
 170 Coastal Current (Fiuza et al., 1998). The Portugal Current flows equatorward transporting
 171 cooler and less saline waters into the region (Carracedo et al., 2014; Peliz et al., 2009). The
 172 Portugal Coastal Current exists only during the upwelling season from late May/early June to
 173 late September/early October, driven by the northerly winds that transport cold and less saline
 174 upwelled water (jet-like) southward (Criado-Aldeanueva et al., 2006; Folkard et al., 1997) (Fig.
 175 1B). Near Cape São Vicente, a part of the Portugal Coastal Current jets turns eastward under
 176 favorable wind conditions and enters the Gulf of Cadiz flowing along the upper slope toward
 177 the Strait of Gibraltar interacting with the upwelling off Cape Santa Maria (Sanchez and
 178 Relvas, 2003) and affecting the region of Site U1387.

179 The Gulf of Cadiz SSTs have a seasonal behavior observed by Folkard et al. (1997)
 180 through satellite images. Temperatures vary between 22.5 °C (summer) (Fig. 1B) and 16.5 °C
 181 (winter) with a mean value of 19.6 °C (Vargas et al., 2003).

182



183

184 **Figure 1:** A: North Atlantic Ocean with annual mean SSTs (°C) at 0.25-degree resolution as
 185 background (WOA 2023; Reagan et al., 2024). Location of IODP Site U1387 and other
 186 available North Atlantic records discussed in the text (IODP Site U1385; ODP Site 980; ODP
 187 Site 1058; DSDP Site 607/IODP Site U1313). Black arrows represent the surface circulation:
 188 GS – Gulf Stream; NAC – North Atlantic Current; PC – Portugal Current; CC – Canary
 189 Current; AzC – Azores Current; NEC – North Equatorial Current; AnC – Antilles Current.
 190 B: Close-up of the study area with locations of IODP Site U1387 and SW Iberian Margin IODP
 191 Sites U1385 and U1391 with the mean summer (July-September) SSTs (°C) at 0.25-degree
 192 resolution as background (WOA 2023; Reagan et al., 2024). Black arrows represent the surface
 193 circulation: AzCC – Azores Countercurrent; IPC – Iberian Poleward Current. Currents adapted
 194 from Baptista et al. (2021) and references therein. Background maps made with ODV
 195 (Schlitzer, 2023).



196 **3. Material and Methods**

197 IODP Site U1387 (36°48.3210'N, 7°43.1321'W) was drilled in December 2011 by the
198 Integrated Ocean Drilling Program (IODP) during Expedition 339 - Mediterranean Outflow
199 into the Faro Drift, northern Gulf of Cadiz, at a water depth of 559 m (Fig. 1) (Expedition 339
200 Scientists, 2013). The samples were collected at a resolution of 12-13 cm along the revised
201 splice (Voelker et al., 2018), except for the interval of Termination X where the resolution was
202 increased to 6-7 cm for the Bajo et al. (2020a) study. Each sample was freeze-dried, weighted
203 and washed through a 63 µm-mesh sieve, following the procedure established in the
204 Sedimentology and Micropaleontology Laboratory of the Division for Geology and Marine
205 Georesources at the Portuguese Institute for the Sea and Atmosphere (IPMA) (Voelker et al.,
206 2015). The coarse fraction residue was transferred onto filter paper, dried at 40 °C, and
207 weighted.

208

209 **3.1 Stable isotope measurements**

210 To establish a stable oxygen isotope record for the chronostratigraphy, 6-12 specimens
211 of the planktonic foraminifera *Globigerinoides bulloides* were collected from the fraction >250
212 µm of a total of 706 samples. The specimens were sent to the gas isotope ratio mass
213 spectrometry laboratory at MARUM (University Bremen), Germany, where they were
214 analyzed with a Finnigan MAT-251 or MAT-252 mass spectrometer coupled to an automated
215 Kiel I or Kiel III carbonate preparation system, respectively. The mass spectrometers' long-
216 term precision is ±0.07 ‰ for δ¹⁸O based on repeated analyses of internal (Solnhofen
217 limestone) and external (NBS-19) carbonate standards. Some of the isotope results were
218 already published in Bajo et al. (2020a) and are available as Bajo et al. (2020b), although the
219 age model used in the current study differs from those data.

220

221 **3.2 Planktonic foraminifer assemblage analysis and SST calculations**

222 For the planktonic foraminifera assemblage, a total of 356 samples were analyzed at a
223 sample resolution of 24-25 cm. Each sample was dry sieved to obtain the fractions >250 µm
224 and 150-250 µm. The respective fraction was then split until about 200 specimens remained in
225 the fraction >250 µm and about 100 specimens in the 150-250 µm fraction. Specimens,
226 including identifiable fragments, were counted, and identified in full in each sub-split.

227 Species identification followed Kučera (2007) and Schiebel and Hemleben (2017). All
228 sinistral coiling *Neogloboquadrina pachyderma* specimens were assigned to *N. pachyderma*,
229 in agreement with the observed morphotypes being similar to those typically found in polar



230 regions (supplementary figure 1). We are using the percentage of *N. pachyderma* to identify
231 cold water incursions of subpolar origin into the Gulf of Cadiz. The assemblage data were
232 converted into relative abundances (percentages) and species grouping into
233 tropical/subtropical, transitional, subpolar/polar habitats according to Kučera (2007). The
234 Azores Current factor was calculated following Salgueiro et al. (2008) and combines the
235 percentages of *Globorotalia inflata*, *Globigerinoides ruber* (white) and *Trilobatus sacculifer*.

236 To evaluate changes related to the subtropical gyre influence, we used the newly
237 developed proxy of the coiling direction of planktonic foraminifera *G. truncatulinoides*, which
238 is a subsurface dwelling species with five morphotypes. The morphotype type II is exclusive
239 of the Atlantic Ocean and the Mediterranean Sea and is the only type with dextral and sinistral
240 forms (de Vargas et al., 2001; Ujiie et al., 2010). According to Billups et al. (2016), the amount
241 of sinistral coiling direction of this species increases when the subtropical gyre circulation is
242 more intense. For this, we analyzed whenever possible all the individuals in the fraction >250
243 μm in all the samples where this species was found (total of 332 samples). Intervals with a high
244 sample volume were split before size fractioning. The coiling ratio was obtained using the
245 following formula: $\% \text{GTS} = \text{GTS} * 100 * (\text{GTS} + \text{GTD})^{-1}$ where GTS is the number of sinistral
246 specimens and GTD the number of dextral specimens (Billups et al., 2016; Ducassou et al.,
247 2018).

248 Using the relative abundance data in the assemblages, we estimated the SST for winter
249 and summer using the non-distance-weighted (ndw) option of the SIMMAX program
250 (Pflaumann et al., 1996), similar to the Modern Analog Technique (MAT), following Salgueiro
251 et al. (2014). Although Jonkers and Kučera (2019) recently showed that only 10 species
252 dominate the SST calculations, we used the complete set of 27 species utilized by Pflaumann
253 et al. (1996) to be consistent with previous reconstructions in the region (Salgueiro et al., 2014;
254 Salgueiro et al., 2010). SST was calculated using 10 nearest neighbors and the modern analog
255 database compiled by Salgueiro et al. (2014), which combines the North Atlantic database of
256 the MARGO project (Kučera et al., 2005) with additional samples for the Iberian Margin
257 (Salgueiro et al., 2008) and off NW Africa (Salgueiro et al., 2014; Voelker and Salgueiro,
258 2017).

259

260 3.3 Alkenone SST reconstructions

261 We also reconstructed SSTs based on the alkenone $U^{K'}_{37}$ index. Alkenones are lipid
262 molecules that are synthesized by coccolithophorid (phytoplankton) and can be extracted from
263 marine sediments using organic solvents. Lipid molecules analyses were done at 24-25 cm



264 resolution (same levels as planktonic foraminifera assemblage data), except for Termination X
265 where the resolution increased to 6-7 cm (Bajo et al., 2020c). Lipid biomarker extraction was
266 done in 338 samples, whereby the SST for the 216 samples between 212.3 and 257.9 c-mcd
267 were already published in Bajo et al. (2020a). Extraction of lipid molecules from freeze-dried
268 sediments followed the procedure established in the DivGM's Biogeochemistry Laboratory
269 (Rodrigues et al., 2017; Voelker et al., 2015), which is based on Villanueva et al. (1997). The
270 di-, tri- and tetra-unsaturated alkenones of 37 carbon atoms were analyzed in a Varian Gas
271 chromatograph Model 3800 equipped with a septum programmable injector and a flame
272 ionization detector (GC-FID) with a CPSIL-5 CB column. Hydrogen was used as carrier gas
273 at a flow rate of 2.5 ml/min and n-hexatriacontane as an internal standard to determine
274 concentrations. To estimate SST's, we used the $U^{K'}_{37}$ index based on the di- and tri-unsaturated
275 alkenones ratio and converted it into temperature values using the global core top calibration
276 of Müller et al. (1998), with an analytical uncertainty of ± 0.5 °C.

277

278 4. Chronostratigraphy and age models

279 One goal of IODP Expedition 339 was always to use the open ocean records from Site
280 U1385 to establish age models for the contourite sites, which are potentially affected by current
281 sorting and tectonics (Hernández-Molina et al., 2016a) and are too shallow to record a global
282 ocean benthic $\delta^{18}O$ signal. So, for contourite sites like IODP Site U1387 the planned approach
283 was to correlate their *G. bulloides* $\delta^{18}O$ surface water record with the one of Site U1385 and
284 thus to transfer the U1385 age model(s) to the contourite site, under the assumption that those
285 records would be similar in such a narrow region affected by the same surface water masses.
286 That approach was followed in this study using the high-resolution *G. bulloides* $\delta^{18}O$ record
287 (Hodell et al., 2023b) published by Hodell et al. (2023a) as correlation target for the Site U1387
288 record. One of the age models of Site U1385 was established by tuning its benthic $\delta^{18}O$ record
289 (Hodell et al., 2023a) to the benthic LR04 stack (Lisiecki and Raymo, 2005), whereas an
290 alternative age model applied tuning to the Probstack (Ahn et al., 2017). The age model used
291 throughout this manuscript for Site U1387 uses the LR04 related ages, although, following
292 Hodell et al. (2023b), Probstack based ages (supplementary figure 2) will also be provided with
293 the data uploaded to the PANGAEA world data center. For MIS boundaries we follow Lisiecki
294 and Raymo (2005) and for MIS substage nomenclature Railsback et al. (2015).

295

296

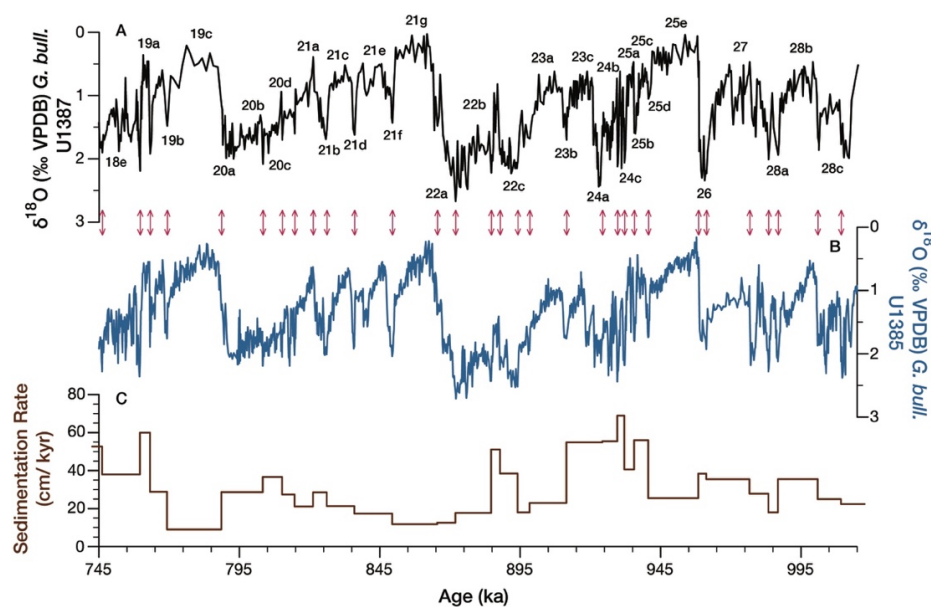
297



298 **5. Results**

299 **5.1 *G. bulloides* $\delta^{18}\text{O}$ record and chronostratigraphy**

300 Besides the glacial-interglacial cycles of MIS 28 to MIS 18, the *G. bulloides* $\delta^{18}\text{O}$ record
301 of Site U1387 reveals millennial-scale stadial-interstadial oscillations, especially following
302 interglacial MIS 25e, MIS 21g, and MIS 19c (Fig. 2A). Notably, an interstadial event occurs
303 within MIS 22 that is also well captured in the Corchia cave $\delta^{18}\text{O}$ record (Bajo et al., 2020a).
304 Overall, the record mimics the one of Site U1385 facilitating the tuning and age model
305 transference (Fig. 2; supplementary fig. 2). The resulting age model for Site U1387 reveals that
306 sedimentation rates were lower during the interglacial intervals dropping to values around 10
307 cm kyr^{-1} (MIS 19c, MIS 21g), whereas they increased during transitional and glacial periods
308 (Fig. 2C). The same pattern in sedimentation rates is generally observed for the Probstack based
309 age model (supplementary figure 2), although age ranges are shifted towards younger ages in
310 the MIS 21 to MIS 28 interval and there occurs an interval with higher sedimentation rates in
311 early MIS 26.
312



313

314 **Figure 2:** A: $\delta^{18}\text{O}$ (‰) *G. bulloides* from IODP Site U1387 and Marine Isotopic Stages and
315 Substages. B: $\delta^{18}\text{O}$ (‰) *G. bulloides* from IODP Site U1385 on its LR04 related age model
316 (Hodell et al., 2023b). Arrows between A and B indicate the tuning points between the two
317 records. C: Sedimentation rates (cm/kyr) for IODP Site U1387.

318



319 **5.2 Planktonic foraminifera fauna**

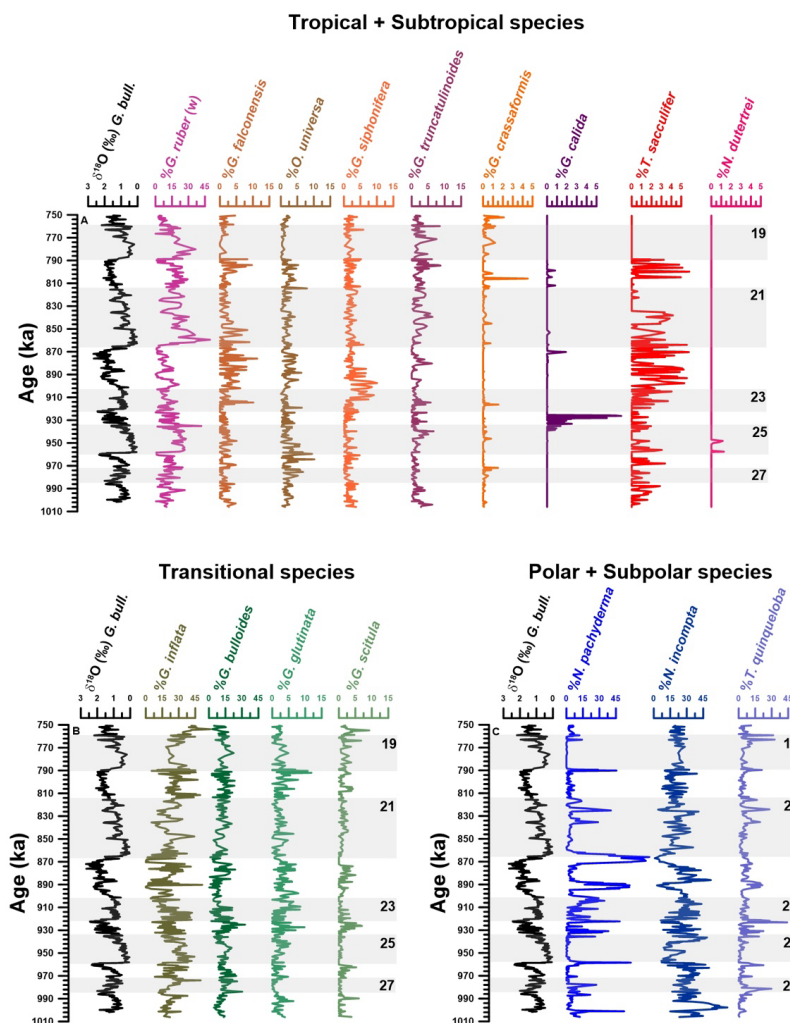
320 At Site U1387, we found faunal assemblages composed by a mix of species from polar,
 321 subpolar, transitional, subtropical, and tropical provinces (Table 1). In total, 16 species were
 322 identified (Table 1; Fig. 3), with the diversity of the subtropical fauna appears to be diminished
 323 due to the absence of *Globoturborotalita tenella*, *Globoturborotalita rubescens*, and
 324 *Globorotalia hirsuta*. Although occurring in low percentages, all three species are present in
 325 surface and Holocene aged sediments of the southwestern Portuguese margin and in the Gulf
 326 of Cadiz (e.g., Ducassou et al., 2018; Rufino et al., 2022; Salgueiro et al., 2008), and both
 327 *Globoturborotalita tenella* and *Globoturborotalita rubescens* have been observed in MIS 19
 328 and younger sediments at Site U1385 (Girone et al., 2023; Martin-Garcia et al., 2015).

329

330 **Table 1** Species found at IODP Site U1387 and the respective provinces. * indicates species
 331 associated with the Azores Current by Storz et al. (2009).

Province	Species
Polar	<i>Neogloboquadrina pachyderma</i>
Subpolar	<i>Neogloboquadrina incompta</i>
	<i>Turborotalita quinqueloba</i> *
Transitional	<i>Globorotalia inflata</i> *
	<i>Globorotalia scitula</i> *
	<i>Globigerinita glutinata</i> *
	<i>Globigerina bulloides</i> *
Subtropical	<i>Globigerinella calida</i>
	<i>Globigerinella siphonifera</i> *
	<i>Globigerinoides ruber (white)</i> *
	<i>Neogloboquadrina dutertrei</i>
	<i>Globorotalia truncatulinoides</i> *
	<i>Globigerina falconensis</i> *
Tropical	<i>Orbulina universa</i>
	<i>Trilobatus sacculifer</i> *
	<i>Globorotalia crassaformis</i>

332



333

334 **Figure 3:** Planktonic foraminifera assemblage from IODP Site U1387. $\delta^{18}\text{O}$ *G. bulloides*
 335 record (‰ VPDB) (black) provided in all three panels as stratigraphic reference. A: Abundance
 336 (%) of tropical species (*Trilobatus sacculifer*; *Globorotalia crassaformis*) and subtropical
 337 species (*Globigerinella siphonifera*; *Globigerinoides ruber* (white); *Neogloboquadrina*
 338 *dutertrei*; *Globigerinella calida*; *Orbulina universa*; *Globigerina falconensis*; *Globorotalia*
 339 *truncatulinoides*). B: Abundance (%) of transitional species (*Globorotalia inflata*;
 340 *Globorotalia scitula*; *Globigerinita glutinata*; *Globigerina bulloides*). C: Abundance (%) of
 341 polar species (*Neogloboquadrina pachyderma*) and subpolar species (*Neogloboquadrina*
 342 *incompta*; *Turborotalita quinqueloba*). Gray bars mark odd-numbered MIS, which include the
 343 interglacial periods. Note, differing y-axis scales.

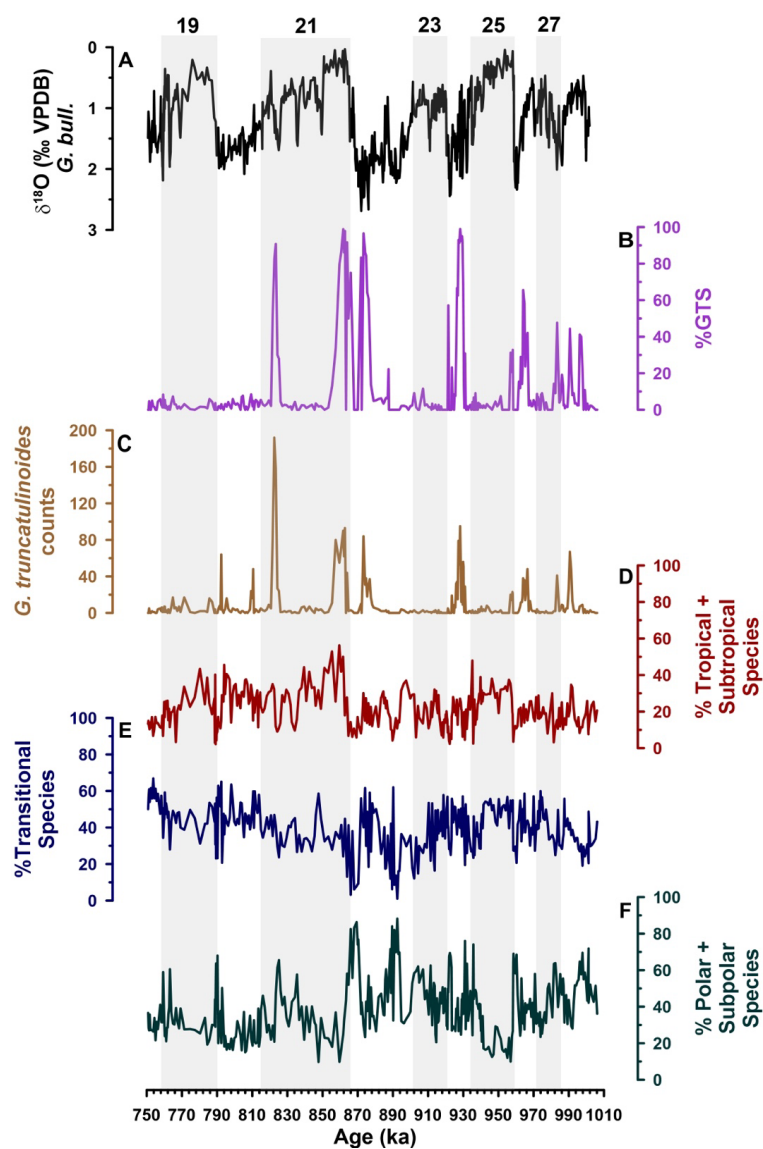


344 Among all species found, only seven have average abundances greater than 2% over
345 the period studied, i.e. *N. pachyderma*, *N. incompta*, *G. inflata*, *G. ruber* (white), *T.*
346 *quinqueloba*, *G. bulloides*, and *G. glutinata* (Fig. 3). These seven species are among the top 10
347 ranked by importance for transfer function models (Jonkers and Kučera, 2019). Two additional
348 species from the top 10 list (*T. sacculifer*, *N. dutertrei*) are present in the samples, but with an
349 abundance of less than 2 %, and one (*G. ruber* pink) is absent. In summary, the results show
350 an alternation of dominance between cold, transitional and warm species through MIS 28 to
351 MIS 18 representing changing conditions in the North Atlantic subtropical gyre.

352 In general, the transitional group is the more abundant one, with an average abundance
353 of 40.3 %, followed by the polar-subpolar group, 38.8 %, and finally the tropical-subtropical
354 group, 20.2 % (Fig. 4; supplementary table 1). The transitional group is present throughout the
355 studied interval but exhibits behavior like the tropical-subtropical group, i.e. low percentages,
356 during some events when the polar-subpolar group dominates the assemblage. Throughout
357 most of the warm periods of the record, the dextral form of the subtropical species *G.*
358 *truncatulinoides* dominates the coiling ratio (% GTS), with a range between 98 and 100 % (Fig.
359 4B). The first interval with increased contributions of the *G. truncatulinoides* sinistral form to
360 the total of *G. truncatulinoides* specimens occurred between 997.8 to 989.9 ka (2.4-44.4 %)
361 followed by seven other events: 986.8 to 981.5 ka (4-47.7 %); 966.6 to 961.6 ka (11.9-65.5
362 %); 958.2 to 956.9 ka (20.6-32.8 %); 930.3 to 925.1 ka (7.6-98.9 %); 887.5 to 873.3 ka (3.3-
363 96.9 %), followed by a short one from 871.9 to 870.3 ka (14.3-83.3 %); a double peak from
364 867 to 863.9 ka (40-91.7 %) and 862.7 to 855.4 ka (13.1-98.9 %); and finally 825.2 to 821.6
365 ka (27.9-90.8 %) (Fig. 4B). During most of those %GTS maxima, the relative abundance of *G.*
366 *truncatulinoides* in the assemblages increased as well (Fig. 3).

367

368



369

370 **Figure 4:** Site U1387 faunal provinces and *Globorotalia truncatulinoides* results. A: $\delta^{18}\text{O}$ (‰)

371 *G. bulloides*. B: *G. truncatulinoides* coiling ratio expressed as % of *G. truncatulinoides*

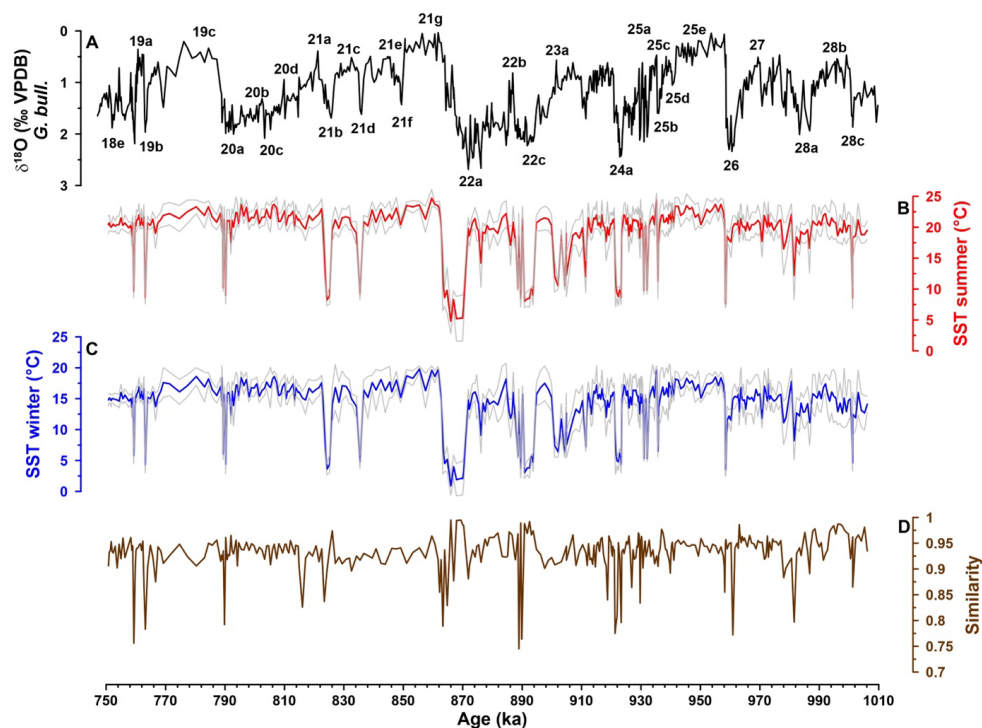
372 (sinistral). C: Number of *G. truncatulinoides* specimens counted in the fraction >250 μm and

373 used to calculate the coiling ratio in C. D: Abundance (%) summed up for Tropical and

374 Subtropical species. E: Abundance (%) of Transitional species. F: Abundance (%) of Polar and

375 Subpolar species. Grey bars mark the odd-numbered MIS.

376



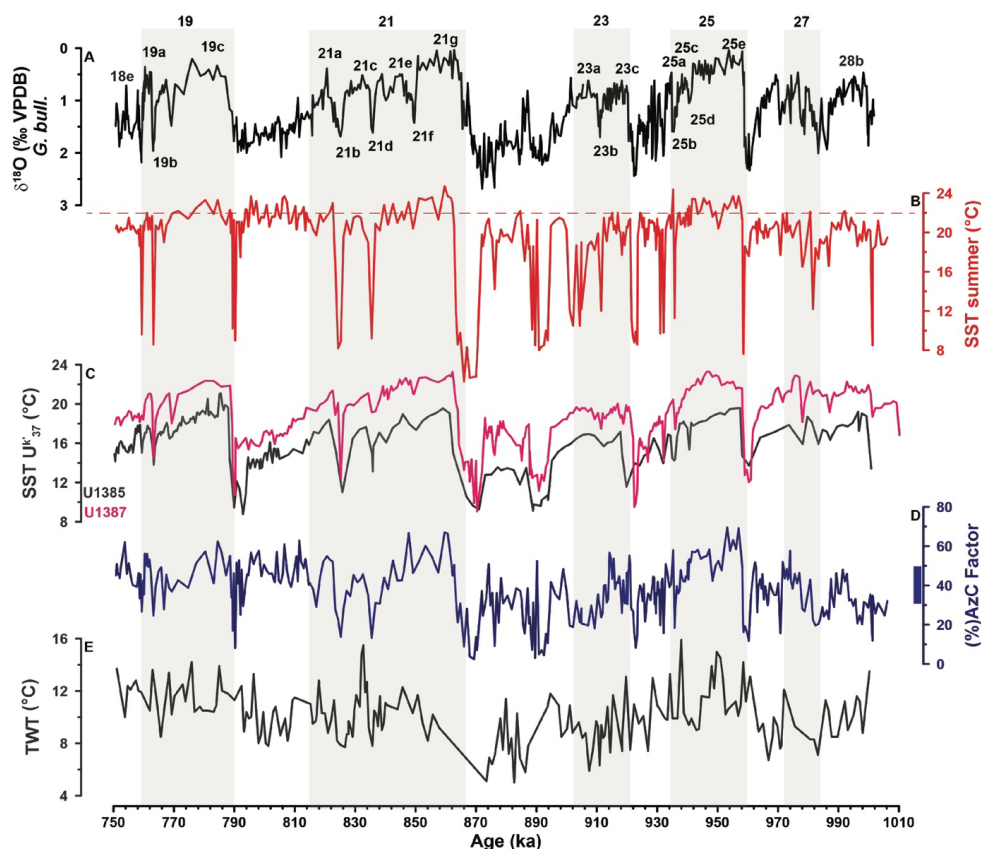
377

378 **Figure 5:** IODP Site U1387 planktonic foraminifera derived SST records A: $\delta^{18}\text{O}$ *G. bulloides*
 379 (‰ VPDB) with numbered Marine Isotopic Stages and Substages. B: Summer SSTs ($^{\circ}\text{C}$) with
 380 standard deviation (1σ). C: Winter SSTs ($^{\circ}\text{C}$) with standard deviation (1σ). D: Similarity to
 381 modern analogs used to calculate the SSTs.

382

383 5.3 Sea-Surface Temperatures

384 The SSTs from IODP Site U1387 estimated with the planktonic foraminifera
 385 assemblage (PF-SST) do not reflect a clear pattern for interglacial-glacial cycles from MIS 28
 386 to MIS 18. Although winter SSTs varied between 0.9 to 19.8 $^{\circ}\text{C}$ and summer SSTs between
 387 4.8 to 24.7 $^{\circ}\text{C}$ (Fig. 5), temperatures remained elevated and relative stable during long periods
 388 with an average of 14.3 $^{\circ}\text{C}$ for winter and of 19.4 $^{\circ}\text{C}$ for summer, excluding the extreme cold
 389 events. Those conditions were interrupted by extreme short cold events when the percentage
 390 of polar and subpolar species increased (Fig. 4F), and winter SSTs dropped below 5 $^{\circ}\text{C}$ (Fig.
 391 5C). Such events occurred within the following MIS substages: 28c; 28a; 26; 25b; 25a; 24c;
 392 24a; 23b; 23a; 22c; 22a; 21d; 21b; 20a; and 19b. The error (1σ) for the winter SSTs ranges
 393 from 0.2 to 4.8 $^{\circ}\text{C}$ and for the summer SSTs from 0.3 to 5.4 $^{\circ}\text{C}$, with the larger errors associated



394

395 **Figure 6:** Comparing Site U1387 and Site U1385 temperature records. A: $\delta^{18}\text{O}$ *G. bulloides*
 396 record of IODP Site U1387 (‰ VPDB) with MIS and substages indicated. B: Planktonic
 397 foraminifera Summer SSTs (°C) from Site U1387 with the dashed line marking the late
 398 Holocene level of 22°C. C: Alkenone derived SST record of IODP Site U1387 (magenta; Bajo
 399 et al., 2020a and this study) in comparison to the Site U1385 record (dark grey; Rodrigues et
 400 al., 2017; Rodrigues et al., 2020). D: The Azores Current factor (%) from IODP Site U1387
 401 with the bar next to the scale indicating the modern range in Gulf of Cadiz surface samples
 402 (Salgueiro et al., 2008). E: Thermocline water temperature (TWT) at Site U1385 (Bahr et al.,
 403 2018; Bahr et al., 2017). Grey bars mark the odd-numbered MIS.

404

405 with those samples with lower similarity values (Fig. 5). The similarity between the respective
 406 Site U1387 sample and the selected 10 modern analog database samples used to estimate the
 407 temperatures is generally above 0.9. Some samples, often associated with extreme cold events,
 408 have a lower similarity between 0.9 and 0.75 (Fig. 5D). At these specific lower similarity



409 samples, we observe a small contribution of "warm" species in a dominantly "cold" assemblage
410 leading to a non-analog situation. The species mix and consequently reduced similarity could
411 be linked to bioturbation and/or current transport in those contourite layers (Expedition 339
412 Scientists, 2013) or to the presence of *N. pachyderma* variants with different temperature
413 affinities (see discussion in subchapter 6.3).

414 The alkenone SSTs (U^{k}_{37} -SST) record with annual temperatures ranging from 9.05 to
415 23.3 °C shows a clear glacial/interglacial cycle pattern (Fig. 6). Despite the differences in
416 amplitudes, both techniques registered the extreme cold events contemporaneously,
417 corroborating the interpretation of these results. The coldest period was recorded at the end of
418 MIS 22 between 870.3 and 864.3 ka. During this period, we recorded the highest percentage
419 of *N. pachyderma* (75.5 %) and the lowest temperatures with PF-SST of 4.8 °C for summer
420 and 0.9 °C for winter and U^{k}_{37} -SST of 9.05 °C.

421

422 6. Discussion

423 6.1 Persisting subtropical gyre influence

424 The strong influence of the AzC in the region is evident through the comparison
425 between the modern planktonic foraminifera assemblage composition (Salgueiro et al., 2008;
426 Rufino et al., 2022) and the reconstructed assemblages from Iberian margin sediments (Girone
427 et al., 2023; Martin-Garcia et al., 2015; Salgueiro et al., 2010; Voelker et al., 2009). During the
428 EMPT, the interglacial and interstadial stages recorded the warmest temperatures, associated
429 with higher percentages of tropical, subtropical and transitional species (Fig. 3; 4D, E).
430 According to Salgueiro et al. (2008), high abundances of *G. ruber* (white), *T. sacculifer* and *G.*
431 *inflata* at the Iberian margin are indicative of the presence of the AzC's eastern branch (AzC
432 factor; Fig. 6D), whereas Storz et al. (2009) associated a much larger species group with the
433 AzC within the subtropical gyre (Table 1). The relative warm SSTs depicted throughout most
434 of the records, i.e. summer PF-SST within a range of 21 to 24.7 °C and winter PF-SST within
435 15 to 19.8 °C, is associated with the "AzC fauna" that include species from the transitional and
436 subtropical provinces (Salgueiro et al., 2008; Storz et al., 2009); so, we interpret those periods
437 with combined increased abundances of tropical, subtropical, and transitional species and with
438 values for the AzC factor above 30 % (Fig. 6D) as being under AzC and thus subtropical gyre
439 influence.

440 The persistent abundance of *N. incompta* (Fig. 3), slightly above the mean value of 18
441 % observed in the surface sediments (Salgueiro et al., 2008), also points to Portugal Current
442 contributions to the prevailing surface waters as it is a main contributor to the Portugal Current



443 factor (Salgueiro et al., 2008). Whereas higher abundances of *G. bulloides* during the EMPT
444 interglacial periods at western Iberian Margin Site U1391 (Fig. 1B) are interpreted as high
445 productivity upwelling periods (Singh et al., 2015), the same is not observed at Site U1387.
446 Here the percentages of *G. bulloides* generally remain below the local surface sediment mean
447 value of 34 % (Salgueiro et al., 2008) with no distinct glacial/interglacial variations, although
448 percentages increased during glacial MIS 24 and MIS 22 (Fig. 3). We interpret the *G. bulloides*
449 pattern at Site U1387 more as a temperature response, with limited influence of waters
450 upwelled in the major upwelling cell off Cape Saint Vicente (Fig. 1B) and advected towards
451 Site U1387. Nevertheless, the sporadic presence of *Chaetoceros* resting spores (diatoms)
452 within interglacial MIS 25e and MIS 28b (called MIS 27b in cited reference) document some
453 influence of seasonal upwelling at Site U1387 (Ventura et al., 2017). Interestingly, the rare
454 occurrences of planktonic foraminifera *N. dutertrei* in MIS 25e (Fig. 3) coincide with the
455 presence of the large-diameter marine diatom species *Coscinodiscus asteromphalus* (Ventura
456 et al., 2017), which can form large blooms and would thus be an ideal food source for *N.*
457 *dutertrei* (Schiebel and Hemleben, 2017).

458 The U^k_{37} -SST data show similar patterns to the PF-SSTs with relatively stable
459 temperatures during interglacial and interstadial substages (Fig. 6). In contrast to the PF-SSTs,
460 the U^k_{37} -SSTs (and abundance) reveal a clear cooling trend from the respective interglacial
461 optimum to the subsequent glacial maximum. This different pattern cannot solely be attributed
462 to the U^k_{37} -SSTs reflecting annual mean temperatures instead of seasonal ones like the PF-
463 SSTs. During the last glacial maximum, the tropical and subtropical regions cooled (MARGO
464 project members, 2009; Osman et al., 2021; Tierney et al., 2020), so that we should expect a
465 similar climate sensitivity and cooling also during the EMPT glacial cycles, conform with the
466 U^k_{37} -SST record of Site U1387 and other global records (McClymont et al., 2013; Naafs et al.,
467 2013; Rodrigues et al., 2017). The difference in the reconstructed SST pattern must, therefore,
468 be caused by the planktonic foraminifera fauna itself. While not obvious in the reconstructed
469 PF-SSTs, a decline in the abundance of the AzC species (Fig. 6D), largely driven by declining
470 *G. ruber* (white) contributions (Fig. 3), and a contemporary increase in Portugal Current
471 associated species (*G. inflata*, *N. incompta*; Fig. 3) is evident in all those interglacial-glacial
472 cycles. However, the AzC factor fauna (Fig. 6D) and other species linked to subtropical gyre
473 waters (Fig. 4D) retain relative high percentages, so that the transfer function is looking for
474 modern analogs in relative warm waters to estimate the EMPT faunal derived SSTs. Thus, due
475 to the faunas being too similar to modern subtropical gyre assemblages (Fig. 5D), the estimated
476 PF-SSTs at Site U1387 appear too warm and do not reflect the global cooling, also expected



477 for the North Atlantic subtropical gyre, during the transitions from the glacial inception to the
478 glacial maximum, at least for the glacial cycles covered by this study. The same pattern is also
479 evident for the PF-SSTs obtained for IODP Site U1385 (Martin-Garcia et al., 2015), which also
480 remained warmer than the corresponding U^{k}_{37} -SSTs (Rodrigues et al., 2017). Site U1387 U^{k}_{37} -
481 SSTs are ~ 2.5 °C warmer than the U^{k}_{37} -SSTs of IODP Site U1385 on the southwestern
482 Portuguese margin (Fig. 1B), but the overall trends are the same (Fig. 6C). A similar
483 temperature difference between both sites is also visible for the PF-SST reconstructions for
484 MIS 21 to MIS 19, i.e. within the interval the records overlap (Martin-Garcia et al., 2015),
485 although the Site U1385 PF-SSTs were obtained using the artificial neural network method and
486 the original MARGO modern analog database from Kučera et al. (2005). We attribute the
487 temperature gradient to a stronger AzC influence at Site U1387, whereas Site U1385 is more
488 affected by the cooler Portugal Current waters (modern annual mean of 16.1 °C).

489 In the Gulf of Cadiz, the summer PF-SSTs and U^{k}_{37} -SSTs reconstructed for the EMPT
490 interglacials were as warm as or slightly warmer than the current interglacial SST (~ 22 °C;
491 Salgueiro et al., 2014) in the case of the warmer interglacials, i.e. MIS 19c, MIS 21g and MIS
492 25e, and 1.5 °C cooler during MIS 23c and MIS 27 (Fig. 6B). However, neither of those
493 interglacial periods experienced surface waters as warm as during early Pleistocene interglacial
494 MIS 47, when U^{k}_{37} -SSTs remained above 24 °C and subtropical planktonic foraminifera
495 abundance mostly above 40 % (Voelker et al., 2022). The warmest EMPT interglacial was MIS
496 21g, supported by high contributions of the subtropical+tropical fauna of up to 56.3 % vs. 45.5
497 % during MIS 19c and 38 % during MIS 25e (Fig. 4), even though MIS 25e received the higher
498 amount of insolation (Rodrigues et al., 2017). The maximum percentages are comparable to
499 those observed during MIS 47 (generally exceeding 40 % and reaching up to 66.8 %), although
500 periods with such high contributions were much shorter during the EMPT interglacials. Much
501 of the subtropical+tropical fauna abundance is driven by the contribution of *G. ruber* (white)
502 (Fig. 3), which can attribute nearly half of the overall percentage. *G. ruber* (white) added less
503 to the MIS 23c fauna (11 %), but this interglacial had a unique fauna due to the higher influence
504 of subtropical species *G. siphonifera* (2.85 %) (Fig. 3) that persisted into MIS 23a when PF-
505 SSTs became less stable caused by the mixture of planktonic foraminifera provinces (including
506 subpolar and polar species).

507 Intra-interglacial SST variability is observed during several of the interglacials because
508 a cooling event was recorded in both SST reconstructions during MIS 21g, MIS 23c and MIS
509 27 leading to a three phased SST evolution, although the timing of the cooling event within the
510 interglacial period varied (Fig. 6). The PF-SSTs documented such a cooling event also for MIS



511 25e, where it occurred prior to the increase in the U^{k}_{37} -SSTs in the younger phase of the
512 interglacial. As such the MIS 25e U^{k}_{37} -SST pattern mimicked the one of MIS 11c on the
513 Portuguese margin (Rodrigues et al., 2011) and in the mid-latitude North Atlantic (Stein et
514 al., 2009), although on a shorter timescale.

515 Recently, Barker et al. (2021) proposed to treat MIS 28 as a "missed" interglacial and
516 we therefore include it in our comparison. The summer PF-SST and U^{k}_{37} -SST records of Site
517 U1387 would support such a notion. Specifically, during interstadial MIS 28b, warm PF-SSTs
518 and U^{k}_{37} -SSTs of 19.6 °C and 21.1 °C, respectively, and considerable contributions of the AzC
519 factor fauna suggest to categorize this period as an interglacial (Fig. 6).

520 Millennial-scale variability in the form of stadial/interstadial oscillations is observed in
521 our records, conform with evidence from other North Atlantic sites, evidencing significant
522 modifications in the North Atlantic's thermohaline circulation, the expansion of continental ice
523 sheets and sea ice, and the atmospheric circulation (e.g., Barker et al., 2021; Billups and
524 Scheinwald, 2014; Hernández-Almeida et al., 2015; Hodell and Channell, 2016; Hodell et al.,
525 2023a; Sun et al., 2021; Rodrigues et al., 2017). At Site U1387, one of the most dynamic
526 periods was the interval between MIS 25 and MIS 22, that points to highly variable surface
527 water conditions in the northern subtropical gyre region, in accordance with evidence from
528 DSDP Site 607 and IODP Site U1313 (Marino et al., 2008; Naafs et al., 2013). Here, we focus
529 on the interstadial periods, with the stadials being discussed later in subchapter 6.3. At Site
530 U1387, the interstadials recorded high mean summer PF-SSTs (20.8 °C) similar to the U^{k}_{37} -
531 SSTs (20.0 °C), and a mean winter PF-SSTs of 15.7 °C. The warmest interstadial according to
532 the summer PF-SSTs was MIS 21e with 23.1 °C, whereas the cooler one reached around 19.9
533 °C (Fig. 5, 6). The interstadials had variable durations with MIS 22b being the longest period
534 with ~16 kyr and MIS 20b the shortest with ~1.5 kyr. Interstadial MIS 22b, occurring during
535 the middle of the glacial MIS 22 and thus within the "900 ka event" period, had a summer PF-
536 SSTs in the general range of 19-21 °C, with the U^{k}_{37} -SSTs being slightly cooler in the 17-18
537 °C range (Fig. 6). During the interstadials of MIS 23, MIS 22, MIS 21, and MIS 20 noteworthy
538 occurrences of the tropical, surface-dwelling species *T. sacculifer* are observed with 1.9 % on
539 average, but increasing to 2.9 % during MIS 21c (Fig. 3). The periods also registered the
540 greatest abundances of the subtropical species *G. falconensis* (average 2.7 %), increasing to 4.6
541 % during interstadial MIS 20b. Those indicator species, together with the higher AzC factor
542 fauna abundance (Fig. 6D), confirm prevailing subtropical gyre water influence and a strong
543 presence of the AzC at the southern Portuguese margin during the interstadials, in accordance
544 with previous observations on the southwestern margin (Girone et al., 2023; Martin-Garcia et



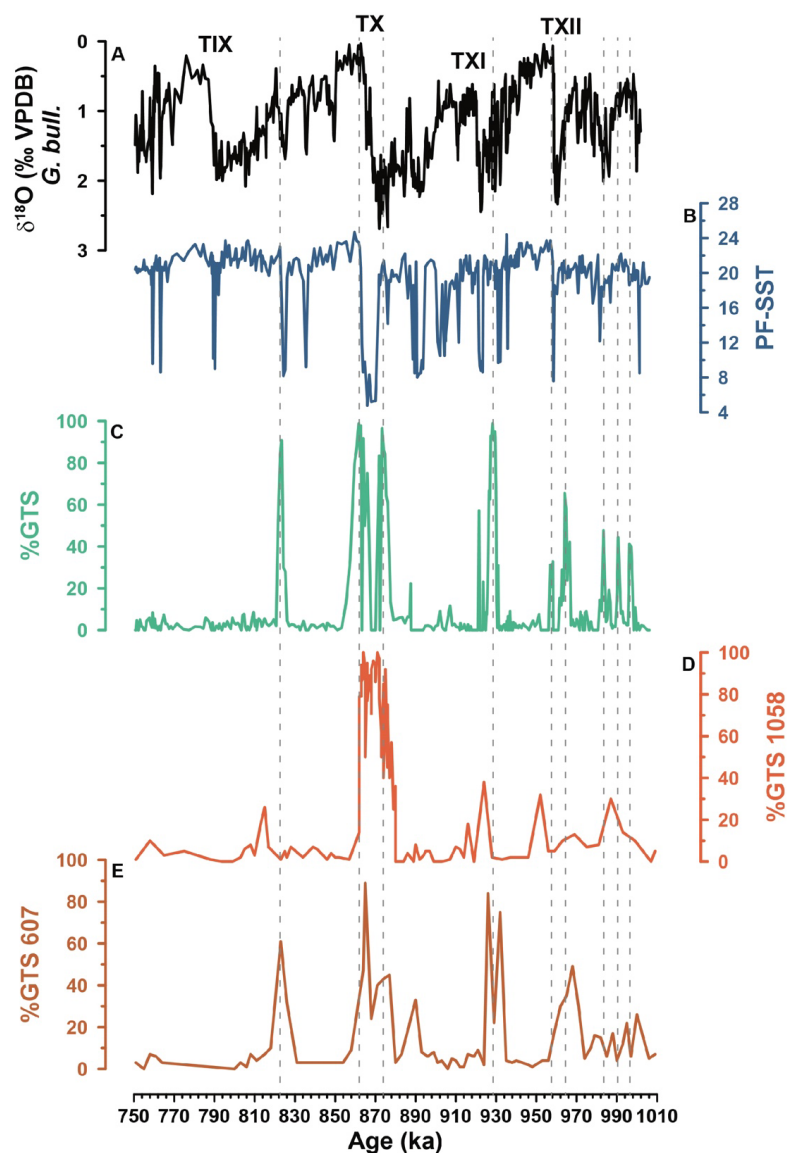
545 al., 2015; Singh et al., 2015). Those warm surface waters were subducted into the thermocline
546 levels and the subtropical North Atlantic Central Water (Bahr et al., 2018). Bahr et al. (2018)
547 link an intensified AzC, coupled to a strong Mediterranean Outflow Water, to their warmer
548 thermocline water temperatures, which is conform with our SST and faunal evidence (e.g., MIS
549 22b, MIS 21c, MIS 19a) (Fig. 6).

550

551 **6.2 *G. truncatulinoides* evidence for subtropical gyre circulation state**

552 *G. truncatulinoides* is a planktonic foraminifera species that prefers relatively warm,
553 nutrient-rich waters such as at the subtropical gyre margins (Ujiié et al., 2010; Rufino et al.,
554 2022). According to Kaiser et al. (2019) and Feldmeijer et al. (2015), the sinistral variant
555 dominates North Atlantic regions with a deep permanent thermocline, such as the central
556 subtropical gyre. Its presence at mid-latitudinal North Atlantic sites, especially during glacial
557 periods, can indicate the northward flux of subtropical waters and thus the position of the gyre's
558 northern boundary (Kaiser et al., 2019). In contrast, *G. truncatulinoides* (dextral) dominates in
559 the Atlantic's tropical waters. High percentages of that variant have been interpreted as
560 reflecting higher contributions of North Equatorial Current and Antilles Current waters to the
561 Gulfstream and thus enhanced westward and northward transport along the western boundary
562 of the subtropical gyre and into its central regions, corresponding with an enhanced gyre
563 circulation overall (Billups et al., 2020).

564 At Site U1387, the dextral variant dominates over the left coiling variant, but is only
565 present in relative low numbers (Fig. 4B, C), comparable to other sites in gyre boundary
566 locations (Kaiser et al., 2019). Nevertheless, the percentage contributions of *G.*
567 *truncatulinoides* to the Site U1387 EMPT faunas (Fig. 3) is in the same range as those observed
568 in surface sediments along the western Iberian margin, in the Gulf of Cadiz and the eastern
569 boundary current region off NW Africa (Salgueiro et al., 2008; Rufino et al., 2022). So, the
570 presence of *G. truncatulinoides*, especially in its right coiling form, supports subtropical gyre
571 influence during much of the studied interval, conform with the evidence discussed above. The
572 foremost characteristics of the *G. truncatulinoides* coiling record are, however, the % GTS
573 maxima during MIS 28, MIS 26, MIS 24, and stadial MIS 21b and a double peak during the
574 period from MIS 22a to MIS 21g (Fig. 4B, 7B). Many of those % GTS peaks have counterparts
575 at northern subtropical gyre Site 607 (Fig. 7D), where those maxima implicate the vicinity of
576 the gyre's northern boundary (Kaiser et al., 2019) and thus a gyre northward expansion not
577 much different from today, in agreement with the relative warm subsurface temperatures



578

579 **Figure 7:** Subtropical gyre intensification episodes. A: $\delta^{18}\text{O}$ (‰) *G. bulloides* from IODP Site

580 U1387. B: summer PF-SST from IODP Site U1387. C: Coiling ratio (%) of planktonic

581 foraminifera *G. truncatulinoides* (sinistral) from IODP Site U1387. D: Coiling ratio (%) of

582 planktonic foraminifera *G. truncatulinoides* (sinistral) from ODP Site 1058 (Kaiser et al.,

583 2019). E: Coiling ratio (%) of planktonic foraminifera *G. truncatulinoides* (sinistral) from

584 DSDP Site 607 (Kaiser et al., 2019). Dashed lines mark peaks of U1387 %GTS maxima.

585 Terminations are indicated by the letter T and the respective Latin numerical.

586



587 reconstructed at the same location (Catunda et al., 2021). Since the total abundance of *G.*
588 *truncatulinoides* (sinistral) increased during most of those periods at Site U1387 as well (Fig.
589 4C), it is possible that the gyre circulation strength was comparable to late Holocene conditions
590 (Billups et al., 2020). Site U1387 recorded % GTS maxima during the MIS 28 and MIS 24 and
591 following the terminal stadial event (Hodell et al., 2015) of Termination XII (MIS 26/ MIS 25),
592 which have no counterparts at Site 607 (Kaiser et al., 2019), at least within the temporal
593 resolution and age model constraints (Fig. 7). Those maxima seem to indicate a vigorous
594 circulation in the eastern region of the subtropical gyre following an (extreme) cold event and
595 might be related to the subtropical gyre expanding northward again when the subarctic front,
596 the boundary between the subpolar and subtropical gyres, receded northward, but was still
597 mostly located south of 41°N, i.e. south of DSDP Site 607.

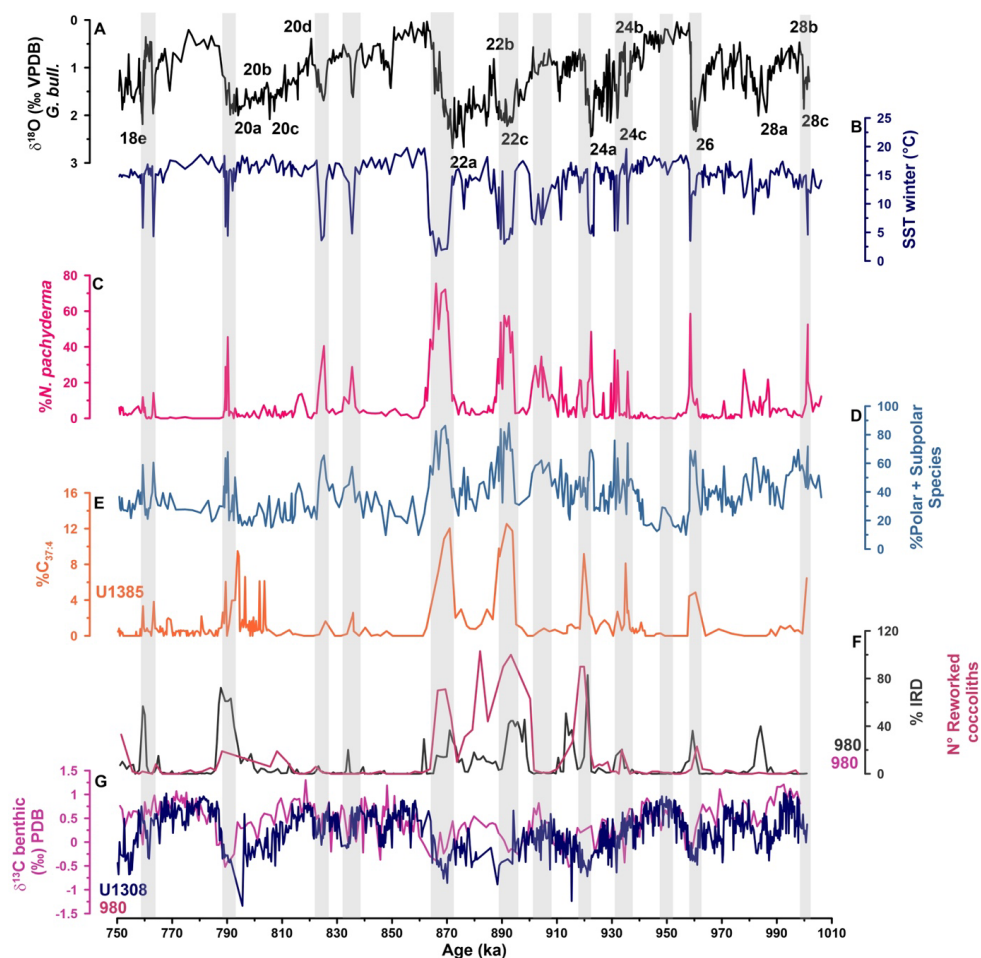
598 The most prominent feature in the % GTS records of Sites U1387, 607 and 1058 is the
599 period from MIS 22a to MIS 21g when % GTS temporarily reached values between 80 to 100
600 % (Fig. 7). At western boundary/Gulf Stream ODP Site 1058 the feature is one long lasting
601 (~20 kyr) peak, whereas both at DSDP Site 607 and IODP Site U1387 a double peak is
602 observed. Based on their Sites 1058 and 607 data, Kaiser et al. (2019) posited that the North
603 Atlantic's subtropical gyre expanded as far north as 41°N (or further) during glacial MIS 22a
604 and that its circulation was more vigorous than during the last glacial maximum. This scenario
605 agrees with the warm subsurface temperatures reconstructed at IODP Site U1313 during MIS
606 22a (Catunda et al., 2021), which were not much cooler than interglacial levels and indicate an
607 expanded layer of subtropical gyre waters. The Site U1387 record now corroborates an
608 expanded and strong subtropical gyre with evidence from the gyre's eastern boundary, i.e., the
609 gyre's eastern boundary must have been located in the vicinity of Site U1387. During the
610 terminal stadial event of Termination X, the subtropical gyre contracted in the north and east
611 leading to the % GTS minima at Sites 607 and U1387 (or even temporary absence of the species
612 at U1387), whereas its western boundary remained near the position of Site 1058 (Kaiser et al.,
613 2019). When the subarctic front receded northward after the terminal stadial event of
614 Termination X, the subtropical gyre expanded again as evidenced by the % GTS maxima at
615 Site 607 and U1387 (Fig. 7), facilitating subtropical water transport to the north and deep-water
616 convection in the North Atlantic (Fig. 8G) (Hodell and Channell, 2016; Hodell et al., 2023a;
617 Kaiser et al., 2019) and the establishment of interglacial conditions.

618
619
620



621 6.3 The extreme cold events

622 Site U1387 recorded several short stadial events (~2 kyr) following the glacial
623 inceptions and as terminal stadial events with winter PF-SSTs dropping to ~5 °C during MIS
624 24a or even to freezing temperatures of 0 °C during MIS 22a (Fig 5, 8B). The U^k_{37} -SSTs during
625 those terminal stadial events also reflect extremely low temperatures, but only reaching 10 °C
626 during MIS 22a and MIS 24a (Fig 6C). The southern position of the subarctic/Arctic front
627 during those stadial periods (Martin-Garcia et al., 2015; Rodrigues et al., 2017), facilitated the
628 presence of the polar species *N. pachyderma*, which reached between 80 % (MIS 22a) and 50
629 % (MIS 24a) (Fig 8C), as well as a general increase in the number of polar and subpolar species
630 (Fig 8D). The high percentages of *N. pachyderma* are much higher than those observed during
631 the Heinrich events of the last glacial cycle in the Gulf of Cadiz (< 20 %) and also exceed those
632 observed in general on the southwestern Portuguese margin during the last 400 kyr (<40 %)
633 (Salgueiro et al., 2014; Salgueiro et al., 2010; Singh et al., 2023; Voelker and De Abreu, 2011).
634 They drive the extremely cold SST estimated for the PF-SST, which appears to introduce a
635 "cold bias" for the winter PF-SST that are much colder than the (annual mean) U^k_{37} -SSTs (Fig.
636 6, 8). The *N. pachyderma* morphotypes (supplementary figure 1) are similar to those found
637 today in the subpolar to polar North Atlantic and those observed in contemporary "middle"
638 Pleistocene sediments in the Alboran Sea (western Mediterranean Sea) (Serrano and Guerra-
639 Merchán, 2012). Although *N. pachyderma* adapted to the colder, polar conditions 1100-1000
640 kyr ago (Huber et al., 2000; Kucera, 2007), thereby establishing the modern polar *N.*
641 *pachyderma* variant (genotype Ia), a recent review of genetic diversity in planktonic
642 foraminifera from the modern global ocean (Morard et al., 2024) revealed that other *N.*
643 *pachyderma* genotypes occur only in lower to mid-latitudinal waters of the Atlantic (e.g., Va,
644 VIa), whereby genotype VIa is well established in the mid-latitudinal North Atlantic, especially
645 in the AzC region, and the Mediterranean Sea. Serrano and Guerra-Merchán (2012) postulated
646 that their early Pleistocene *Neogloboquadrina* specimens from the Alboran Sea might include
647 two groups with different temperature affinities, one being the modern polar variant and the
648 other living in warmer waters and/or upwelling conditions. Their observations indicate that the
649 mid-latitudinal North Atlantic genotype VIa or a precursor of it might have already been
650 present in the early Pleistocene. As it is difficult to distinguish between the genotypes based
651 on morphology, it is possible that the Site U1387 EMPT *N. pachyderma* specimens include
652 both the polar and the mid-latitudinal, warmer water affinity variants. Presence of a warmer
653 water variant would agree with the low, but noticeable contemporary presence of various
654 subtropical species and of tropical species *T. sacculifer* in the Site U1387 faunas (Fig. 3, 4D)



655

656 **Figure 8:** The extreme cold events. A: IODP Site U1387 *G. bulloides* $\delta^{18}\text{O}$ (‰ VPDB) record
 657 with MIS and substages. B: Winter PF-SST (°C) from IODP Site U1387. C: Abundance (%)
 658 of the planktonic foraminifera *N. pachyderma* from IODP Site U1387. D: Abundance (%) of
 659 polar and subpolar species at IODP Site U1387. E: $\%C_{37:4}$ freshwater indicator from IODP Site
 660 U1385 (Rodrigues et al., 2017). F: Number of reworked coccoliths (Marino et al., 2011) and
 661 abundance (%) of ice-rafted debris from ODP Site 980 (Wright and Flower, 2002). G: $\delta^{13}\text{C}$
 662 benthic foraminifera (‰ VPDB) (magenta line) from ODP Site 980 (Wright and Flower, 2002),
 663 and $\delta^{13}\text{C}$ benthic foraminifera (‰) (dark blue line) from IODP Site U1308 (Hodell and
 664 Channell, 2016). Gray bars mark cold events.

665

666 that hint to some AzC/subtropical gyre influence. This is especially true for MIS 22 when such
 667 subtropical water contributions would be consistent with the relative northern expansion of the



668 subtropical gyre (Catunda et al., 2021; Kaiser et al., 2019). Because the modern analog
669 technique used to calculate the PF-SST relies on the percentage contributions of *N. pachyderma*
670 to the total fauna it looks for modern analogs in the Nordic Seas and Labrador Sea and therefore
671 overestimates the cooling, if the % *N. pachyderma* values include relevant contributions of a
672 warm water variant or where that variant dominates. So, for the interpretation of the cold stadial
673 events we give more weight to those events where PF-SSTs and U^k_{37} -SSTs show contemporary
674 cooling and caution that some of the extreme cold PF-SSTs might be overestimated.

675 The terminal stadial events (Fig. 8) are all clearly marked in the PF-SSTs and U^k_{37} -
676 SSTs record with extreme cooling. The Termination X event (MIS 22a) lasted the longest (6
677 kyr) and was the coldest, registering with lowest SSTs of the whole study interval. In contrast
678 to the southwestern Portuguese margin records from Site U1385 (Girone et al., 2023; Rodrigues
679 et al., 2017), southward incursion of cold surface waters to Site U1387 during Termination IX
680 was much more limited as indicated by the diminished cooling in regard to amplitude and
681 duration. When compared to the others, an atypical terminal stadial event occurred at the end
682 of MIS 28a with low *N. pachyderma* abundances (20 %) and relatively warm PF-SST (10 °C)
683 (Fig. 8). The event presents, however, an assemblage dominated by polar and subpolar species
684 (60 %) and evidence of ice-rafting at ODP Site 980 in the subpolar North Atlantic (Fig. 8F)
685 (Wright and Flower, 2002). All terminal stadial events registered at Site U1387 coincided with
686 ice rafting and melting icebergs in the North Atlantic (Fig. 8E, F) (Hodell and Channell, 2016;
687 Marino et al., 2011; Rodrigues et al., 2017; Wright and Flower, 2002) and a related strong
688 reduction of the AMOC depth as evidenced by the presence of AABW in water depths normally
689 occupied by NADW (Fig. 8G) (Hernández-Almeida et al., 2015; Hodell and Channell, 2016;
690 Hodell et al., 2023a). The Site U1387 records, therefore, provide further evidence for an
691 extreme contraction of the subtropical gyre in the eastern North Atlantic during those events
692 and indicate that the subarctic front advanced much further south during those events than
693 during the Heinrich events of the last glacial cycle or any terminal stadial events of the last 400
694 kyr, as already previously suggested by Rodrigues et al. (2017).

695 In addition to the terminal stadial events, there occurred stadial events during MIS 24c,
696 MIS 23b, MIS 21d, MIS 21b, MIS 19b, and MIS 18e with similar environmental characteristics
697 (Fig 8). Although those periods presented lower % *N. pachyderma* between 20 % during MIS
698 18e and 40 % during MIS 24c, the assemblages were dominated by polar and subpolar species
699 (60-80%) resulting in very cold winter PF-SSTs. The transition to the glacial maximum of MIS
700 24 was marked by three stadial/interstadial oscillations, with the first two occurring early on
701 and with only 2 kyr separating them. The last stadial was a little cooler (4.9 °C) but was



702 associated with a strong increase in *N. pachyderma* abundance (50 %) and high amounts of
703 IRD (80 %) and reworked coccoliths (90 %) in the subpolar North Atlantic at the ODP Site
704 980 (Marino et al., 2011; Wright and Flower, 2002) (Fig. 8). This evidence, combined with the
705 lower $U^{k_{37}}\text{-SST}$ (10 °C) at Site U1387 and the presence of freshwater input at Site U1385
706 (Rodrigues et al., 2017), indicate a strong southward displacement of the subarctic front also
707 during this event. The cold events in MIS 23b, MIS 21b and MIS 18e were associated with
708 hardly any cooling in the $U^{k_{37}}\text{-SSTs}$ (Fig. 6), representing potential cases of “cold bias” in the
709 PF-SSTs.

710 The transition between MIS 23 and MIS 22 initiated the “900 ka event”. Cooler
711 temperatures during MIS 23 led to an abrupt increase in Antarctic ice volume and thus lowering
712 of the sea level to 120 m below present (Elderfield et al., 2012). The lower sea level permitted
713 the advance of marine-based ice sheets around the North Atlantic with impacts on ice-rafting
714 and subarctic front movements (Hodell and Channell, 2016). At Site U1387, those background
715 conditions resulted in a cooling event during MIS 23a that is clearly visible in the planktonic
716 foraminifera records, but not the $U^{k_{37}}\text{-SST}$ records of either Site U1387 or Site U1385 (Fig. 4,
717 6, 8). It is, however, contemporary with a short cooling in the subtropical gyre’s subsurface
718 waters at Site U1313 (Catunda et al., 2021). The cooling trend initiated with this event
719 culminated in the first, prolonged period of extreme cold conditions during MIS22c at Site
720 U1387 (Fig. 6, 8). In the mid-latitudinal North Atlantic ice-rafting and iceberg melting (Hodell
721 and Channell, 2016; Marino et al., 2011; Wright and Flower, 2002) led to freshening of the
722 surface waters, even as far south as Site U1385 (Fig. 8E) (Rodrigues et al., 2017), and
723 subsequently to a reduction in the AMOC depth (Fig. 8G) (Hernández-Almeida et al., 2015;
724 Hodell and Channell, 2016; Hodell et al., 2023a; Wright and Flower, 2002). The associated
725 contraction of the subtropical gyre is also reflected in the subsurface waters at Site U1313
726 cooling by 2 °C to the range of 4 °C (Catunda et al., 2021), a cooling that is not seen during
727 MIS 22a when the subtropical gyre was stronger (Kaiser et al., 2019).

728

729 **Conclusions**

730 The planktonic foraminifera faunal and SST records of IODP Site U1387 revealed that
731 subtropical gyre waters, especially those related to the AzC, greatly influenced the Gulf of
732 Cadiz during the EMPT interval from MIS 28 to MIS 18, even during the transitions to full
733 glacial conditions following the glacial inceptions. The planktonic foraminifera fauna includes
734 species from all four provinces with the subpolar and polar species dominating during the
735 extreme cold events, in particular the terminal stadial events. The faunal diversity differed



736 slightly from the Holocene, a topic which implications for ecosystem state and restoration
737 efforts in the region will be explored further in the future. Interglacial periods and several of
738 the interstadials experienced SST as warm or slightly warmer than today and registered
739 persistent AzC influence. The warmest interglacial period was MIS 21g and the coolest, as to
740 be expected from the global climate state, MIS 23. MIS 23 exhibited a particular subtropical
741 planktonic foraminifera fauna, which, in contrast to the other interglacials, included a lesser
742 contribution of *G. ruber* white, but higher ones of *G. falconensis* and *G. siphonifera*.
743 Interestingly, tropical species *T. sacculifer* was present in low percentages throughout MIS 23
744 and even glacial MIS 22, which included the two periods with the coldest SST of the studied
745 time interval.

746 Glacial MIS 22a with the terminal stadial event of Termination X stands out as a special
747 time. On the one hand, the highest % *N. pachyderma* and coldest SST during a prolonged
748 period indicate extreme cooling and incursion of subpolar waters into the latitudes of the Gulf
749 of Cadiz. This is only possible if the subarctic front was shifted southward in the eastern North
750 Atlantic. On the other hand, Kaiser et al. (2019) infer the subtropical gyre expanded at least as
751 far north as 41°N, with a circulation more vigorous than during the last glacial maximum. The
752 % GTS data of Site U1387 agrees with such a scenario and indicates that the eastern boundary
753 of the subtropical gyre was in the vicinity of the Gulf of Cadiz during much of MIS 22a, with
754 the exception of the peak of the terminal stadial event. As such, the Gulf of Cadiz is once again
755 confirmed as an important confluence region during glacial periods.

756 Millennial-scale climate variability is clearly recorded as stadial/interstadial SST
757 oscillations during the transition from MIS 25 to MIS 24, whereas during the MIS 21 to MIS
758 20 transition only MIS 21d and MIS 21b experienced short-term cooling events. Likewise, MIS
759 19b was associated with a short-term cooling event.

760 By combining evidence from planktonic foraminifera assemblages with two types of
761 SST reconstructions, we have identified potential biases in our reconstructions. The persistent
762 presence of subtropical gyre and AzC related species in our samples leads to overestimated PF-
763 SSTs following the glacial inceptions and during part of the glacial periods, which becomes
764 obvious in comparison with the U^k_{37} -SSTs. On the other hand, the “hidden” presence of a *N.*
765 *pachyderma* variant with an affinity to warmer AzC current waters, mixed in with the polar
766 variant, probably leads to a cold bias in the PF-SST reconstructions of the extreme cold events.
767 The temporal evolution of *N. pachyderma* and its affinities and potential implications for
768 paleoceanographic reconstructions in the region will be explored in the future, when the Site
769 U1387 planktonic foraminifera faunal records going back to 1500 ka have been completed.



770

771 **Data availability.** *G. bulloides* oxygen isotope and $U^{k'}_{37}$ SST raw data for MIS 21-MIS 26
772 were already published in Bajo et al. (2020a); note that Bajo et al. (2020b, c) ages listed in
773 Pangaea differ from the age model used in this manuscript:

774 <https://doi.pangaea.de/10.1594/PANGAEA.914401>

775 <https://doi.pangaea.de/10.1594/PANGAEA.914400>

776 Data published in this manuscript will also be archived at Pangaea (to be submitted as soon as
777 the preprint is published and the manuscript has a doi) and are currently provided as
778 supplementary material for the review process.

779

780 **Supplement.** The supplement related to this article is available online at:.....

781

782 **Author contributions.** AHLV initiated and designed the study and secured funding for the
783 biogeochemical and stable isotope analyses. AM produced the planktonic foraminifera faunal
784 data and, together with AHLV, wrote the first draft of the manuscript. ES trained AM in the
785 application of SIMMAX and the interpretation of its results. MP produced the lipid biomarker
786 data under the supervision of TR who also made the final quality control of the results. HK
787 performed the stable isotope analyses at MARUM. All authors, with the exception of MP, who
788 left science in the meantime, read and commented on the draft of the manuscript and approved
789 its final version.

790

791 **Competing interests.** At least one of the (co-)authors is a member of the editorial board of
792 *Climate of the Past*. The authors have no other competing interests to declare.

793

794 **Acknowledgments.** The samples for this study were provided by the Integrated Ocean Drilling
795 Program (2003-2013) and we thank the Bremen Core Repository and its staff for support in
796 sampling the sections. We thank W. Soares, Cremilde Monteiro and the research fellows
797 contracted by the MOWCADYN project for help in preparing the samples in the
798 micropaleontology and sedimentology lab at IPMA.

799

800 **Financial support.** The stable isotope and lipid biomarker analyses were made possible
801 through Fundação para a Ciência e a Tecnologia (FCT) funded R&D project MOWCADYN
802 (PTDC/MAR-PRO/3761/2012). Additional financial support from FCT was provided to the
803 Centro de Ciências do Mar do Algarve (CCMAR) through projects: basic funding



804 UIDB/04326/2020 (<https://doi.org/10.54499/UIDB/04326/2020>); programmatic funding
805 UIDP/04326/2020 (<https://doi.org/10.54499/UIDP/04326/2020>) and the CIMAR associated
806 laboratory funding LA/P/0101/2020 (<https://doi.org/10.54499/LA/P/0101/2020>). A. Mega is
807 funded by FCT/CCMAR through PhD fellowship CCMAR01/UIDP/04326/2020. A. Voelker
808 acknowledges her Investigador FCT grant (IF/01500/2014), which provided her salary during
809 the initial phase of the study (2015-2021). The SEM work was made possible through access
810 to the GOLD lab facilities at IPMA funded by the EMSO-PT infrastructure project (POCI-01-
811 0145-FEDER-022157).

812

813 **References**

- 814 Ahn, S., Khider, D., Lisiecki, L. E., and Lawrence, C. E.: A probabilistic Pliocene–Pleistocene
815 stack of benthic $\delta^{18}\text{O}$ using a profile hidden Markov model, *Dynamics and Statistics of the*
816 *Climate System*, 2, <https://doi.org/10.1093/climsys/dzx002>, 2017.
- 817 Ambar, I., Armi, L., Bower, A., and Ferreira, T.: Some aspects of time variability of the
818 Mediterranean Water off south Portugal, *Deep-Sea Res Pt I*, 46, 1109-1136, 1999.
- 819 Bahr, A., Kaboth, S., Hodell, D., Zeeden, C., Fiebig, J., and Friedrich, O.: Oceanic heat pulses
820 fueling moisture transport towards continental Europe across the mid-Pleistocene transition,
821 *Quaternary Science Reviews*, 179, 48-58, <https://doi.org/10.1016/j.quascirev.2017.11.009>,
822 2018.
- 823 Bahr, A., Kaboth, S., Hodell, D. A., Zeeden, C., Fiebig, J., and Friedrich, O.: Temperature
824 reconstruction for the Mid-Pleistocene Transition based on deep-dwelling foraminifera of
825 IODP Site339-U1385, <https://doi.org/10.1594/PANGAEA.882374>, 2017.
- 826 Bajo, P., Drysdale, R. N., Woodhead, J. D., Hellstrom, J. C., Hodell, D., Ferretti, P., Voelker,
827 A. H. L., Zanchetta, G., Rodrigues, T., Wolff, E., Tyler, J., Frisia, S., Spötl, C., and Fallick,
828 A. E.: Persistent influence of obliquity on ice age terminations since the Middle Pleistocene
829 transition, *Science*, 367, 1235-1239, <https://doi.org/10.1126/science.aaw1114>, 2020a.
- 830 Bajo, P., Drysdale, R. N., Woodhead, J. D., Hellstrom, J. C., Hodell, D. A., Ferretti, P., Voelker,
831 A. H. L., Zanchetta, G., Rodrigues, T., Wolff, E. W., Tyler, J. J., Frisia, S., Spötl, C., and
832 Fallick, A. E.: Oxygen isotope of planktic foraminifera *Globigerina bulloides* from IODP
833 Site 339-U1387, PANGAEA [dataset], <https://doi.org/10.1594/PANGAEA.914401>, 2020b.
- 834 Bajo, P., Drysdale, R. N., Woodhead, J. D., Hellstrom, J. C., Hodell, D. A., Ferretti, P., Voelker,
835 A. H. L., Zanchetta, G., Rodrigues, T., Wolff, E. W., Tyler, J. J., Frisia, S., Spötl, C., and
836 Fallick, A. E.: SST and synchronized ages from IODP Site 339-U1387, PANGAEA
837 [dataset], <https://doi.org/10.1594/PANGAEA.914400>, 2020c.
- 838 Baptista, L., Santos, A. M., Melo, C. S., Rebelo, A. C., Madeira, P., Cordeiro, R., Botelho, A.
839 Z., Hipólito, A., Pombo, J., Voelker, A. H. L., and Ávila, S. P.: Untangling the origin of the
840 newcomer *Phorcus sauciatus* (Mollusca: Gastropoda) in a remote Atlantic archipelago,
841 *Marine Biology*, 168, 1-16, <https://doi.org/10.1007/s00227-020-03808-5>, 2021.
- 842 Barker, S., Zhang, X., Jonkers, L., Lordsmith, S., Conn, S., and Knorr, G.: Strengthening
843 Atlantic Inflow Across the Mid-Pleistocene Transition, *Paleoceanography and*
844 *Paleoclimatology*, 36, e2020PA004200, <https://doi.org/10.1029/2020PA004200>, 2021.
- 845 Barker, S., Knorr, G., Edwards, R. L., Parrenin, F., Putnam, A. E., Skinner, L. C., Wolff, E.,
846 and Ziegler, M.: 800,000 Years of Abrupt Climate Variability, *Science*, 334, 347-351,
847 <https://doi.org/10.1126/science.1203580>, 2011.



- 848 Barker, S., Starr, A., van der Lubbe, J., Doughty, A., Knorr, G., Conn, S., Lordsmith, S., Owen,
849 L., Nederbragt, A., Hemming, S., Hall, I., Levay, L., null, n., Berke, M. A., Brentegani, L.,
850 Caley, T., Cartagena-Sierra, A., Charles, C. D., Coenen, J. J., Crespin, J. G., Franzese, A.
851 M., Gruetzner, J., Han, X., Hines, S. K. V., Jimenez Espejo, F. J., Just, J., Koutsodendris,
852 A., Kubota, K., Lathika, N., Norris, R. D., Periera dos Santos, T., Robinson, R., Rolison, J.
853 M., Simon, M. H., Tanguan, D., Yamane, M., and Zhang, H.: Persistent influence of
854 precession on northern ice sheet variability since the early Pleistocene, *Science*, 376, 961-
855 967, <https://doi.org/10.1126/science.abm4033>, 2022.
- 856 Billups, K. and Scheinwald, A.: Origin of millennial-scale climate signals in the subtropical
857 North Atlantic, *Paleoceanography*, 29, 612-627, <https://doi.org/10.1002/2014PA002641>,
858 2014.
- 859 Billups, K., Hudson, C., Kunz, H., and Rew, I.: Exploring *Globorotalia truncatulinoides*
860 coiling ratios as a proxy for subtropical gyre dynamics in the northwestern Atlantic Ocean
861 during late Pleistocene Ice Ages, *Paleoceanography*, 31, 553-563,
862 <https://doi.org/10.1002/2016PA002927>, 2016.
- 863 Billups, K., Vizcaíno, M., Chiarello, J., and Kaiser, E. A.: Reconstructing Western Boundary
864 Current Stability in the North Atlantic Ocean for the Past 700 Kyr From *Globorotalia*
865 *truncatulinoides* Coiling Ratios, *Paleoceanography and Paleoclimatology*, 35,
866 <https://doi.org/10.1029/2020PA003958>, 2020.
- 867 Carracedo, L. I., Gilcoto, M., Mercier, H., and Pérez, F. F.: Seasonal dynamics in the Azores–
868 Gibraltar Strait region: A climatologically-based study, *Progress in Oceanography*, 122,
869 116-130, <http://dx.doi.org/10.1016/j.pocean.2013.12.005>, 2014.
- 870 Carracedo Segade, L. I., Gilcoto, M., Mercier, H., and Pérez, F. F.: Quasi-synoptic transport,
871 budgets and water mass transformation in the Azores–Gibraltar Strait region during summer
872 2009, *Progress in Oceanography*, 130, 47-64,
873 <http://dx.doi.org/10.1016/j.pocean.2014.09.006>, 2015.
- 874 Catunda, M. C. A., Bahr, A., Kaboth-Bahr, S., Zhang, X., Foukal, N. P., and Friedrich, O.:
875 Subsurface Heat Channel Drove Sea Surface Warming in the High-Latitude North Atlantic
876 During the Mid-Pleistocene Transition, *Geophysical Research Letters*, 48,
877 <https://doi.org/10.1029/2020GL091899>, 2021.
- 878 Chalk, T. B., Hain, M. P., Foster, G. L., Rohling, E. J., Sexton, P. F., Badger, M. P. S., Cherry,
879 S. G., Hasenfratz, A. P., Haug, G. H., Jaccard, S. L., Martínez-García, A., Pälike, H.,
880 Pancost, R. D., and Wilson, P. A.: Causes of ice age intensification across the Mid-
881 Pleistocene Transition, *Proceedings of the National Academy of Sciences*, 114, 13114-
882 13119, <https://doi.org/10.1073/pnas.1702143114>, 2017.
- 883 Clark, P. U.: Ice Sheets in Transition, *Science*, 337, 656-658,
884 <https://doi.org/10.1126/science.1226335>, 2012.
- 885 Clark, P. U., Shakun, J. D., Rosenthal, Y., Köhler, P., and Bartlein, P. J.: Global and regional
886 temperature change over the past 4.5 million years, *Science*, 383, 884-890,
887 <https://doi.org/10.1126/science.adi1908>, 2024.
- 888 Clark, P. U., Archer, D., Pollard, D., Blum, J. D., Rial, J. A., Brovkin, V., Mix, A. C., Pisias,
889 N. G., and Roy, M.: The middle Pleistocene transition: characteristics, mechanisms, and
890 implications for long-term changes in atmospheric pCO₂, *Quaternary Science Reviews*, 25,
891 3150-3184, 2006.
- 892 Criado-Aldeanueva, F., Garcia-Lafuente, J., Vargas, J. M., Del Rio, J., Vazquez, A., Reul, A.,
893 and Sanchez, A.: Distribution and circulation of water masses in the Gulf of Cadiz from in
894 situ observations, *Deep Sea Research Part II: Topical Studies in Oceanography*, 53, 1144-
895 1160, <https://doi.org/10.1016/j.dsr2.2006.04.012>, 2006.



- 896 Curry, W. B. and Oppo, D. W.: Glacial water mass geometry and the distribution of $\delta^{13}\text{C}$ of
897 ΣCO_2 in the western Atlantic Ocean, *Paleoceanography*, 20,
898 <https://doi.org/10.1029/2004PA001021>, 2005.
- 899 de Vargas, C., Renaud, S., Hilbrecht, H., and Pawlowski, J.: Pleistocene adaptive radiation in
900 *Globorotalia truncatulinoides*: genetic, morphologic, and environmental evidence,
901 *Paleobiology*, 27, 104-125, [https://doi.org/10.1666/0094-
902 8373\(2001\)027<0104:PARIGT>2.0.CO;2](https://doi.org/10.1666/0094-8373(2001)027<0104:PARIGT>2.0.CO;2), 2001.
- 903 Ducassou, E., Hassan, R., Gonthier, E., Duprat, J., Hanquiez, V., and Mulder, T.:
904 Biostratigraphy of the last 50 kyr in the contourite depositional system of the Gulf of Cádiz,
905 *Marine Geology*, 395, 285-300, <https://doi.org/10.1016/j.margeo.2017.09.014>, 2018.
- 906 Elderfield, H., Ferretti, P., Greaves, M., Crowhurst, S., McCave, I. N., Hodell, D., and
907 Piotrowski, A. M.: Evolution of Ocean Temperature and Ice Volume Through the Mid-
908 Pleistocene Climate Transition, *Science*, 337, 704-709, [10.1126/science.1221294](https://doi.org/10.1126/science.1221294), 2012.
- 909 Expedition 339 Scientists: Site U1387, in: *Proceedings IODP Exp. 339 - Mediterranean*
910 *Outflow*, edited by: Stow, D. A. V., Hernández-Molina, F. J., Alvarez Zarikian, C. A., and
911 the Expedition 339 Scientists, Integrated Ocean Drilling Program Management
912 International, Inc., Tokyo, <https://doi.org/10.2204/iodp.proc.339.105.2013>, 2013.
- 913 Eynaud, F., de Abreu, L., Voelker, A., Schönfeld, J., Salgueiro, E., Turon, J.-L., Penaud, A.,
914 Toucanne, S., Naughton, F., Sanchez Goni, M. F., Malaize, B., and Cacho, I.: Position of
915 the Polar Front along the western Iberian margin during key cold episodes of the last 45 ka,
916 *Geochem. Geophys. Geosyst.*, 10, <https://doi.org/10.1029/2009GC002398>, 2009.
- 917 Farmer, J. R., Hönisch, B., Haynes, L. L., Kroon, D., Jung, S., Ford, H. L., Raymo, M. E.,
918 Jaume-Seguí, M., Bell, D. B., Goldstein, S. L., Pena, L. D., Yehudai, M., and Kim, J.: Deep
919 Atlantic Ocean carbon storage and the rise of 100,000-year glacial cycles, *Nat Geosci*,
920 <https://doi.org/10.1038/s41561-019-0334-6>, 2019.
- 921 Feldmeijer, W., Metcalfe, B., Brummer, G. J. A., and Ganssen, G. M.: Reconstructing the depth
922 of the permanent thermocline through the morphology and geochemistry of the deep
923 dwelling planktonic foraminifer *Globorotalia truncatulinoides*, *Paleoceanography*, 30, 1-
924 22, <https://doi.org/10.1002/2014PA002687>, 2015.
- 925 Fiuza, A. F. G., Hamann, M., Ambar, I., del Rio, G. D., Gonzalez, N., and Cabanas, J. M.:
926 Water masses and their circulation off western Iberia during May 1993, *Deep-Sea Res Pt I*,
927 45, 1127-1160, 1998.
- 928 Folkard, A. M., Davies, P. A., Fiuza, A. F. G., and Ambar, I.: Remotely sensed sea surface
929 thermal patterns in the Gulf of Cadiz and the Strait of Gibraltar: Variability, correlations,
930 and relationships with the surface wind field, *Journal of Geophysical Research*, 102, 5669-
931 5683, 1997.
- 932 Frouin, R., Fiuza, A. F. G., Ambar, I., and Boyd, T. J.: Observations of a Poleward Surface
933 Current Off the Coasts of Portugal and Spain during Winter, *Journal of Geophysical*
934 *Research*, 95, 679-691, 1990.
- 935 Girone, A., De Astis, A., Sierro, F. J., Hernández-Almeida, I., Garcia, M. A., Sánchez Goñi,
936 M. F., Maiorano, P., Marino, M., Trotta, S., and Hodell, D.: Planktonic foraminifera
937 response to orbital and millennial-scale climate variability at the southern Iberian Margin
938 (IODP Site U1385) during Marine Isotope Stages 20 and 19, *Palaeogeography,*
939 *Palaeoclimatology,* *Palaeoecology*, 615, 111450,
940 <https://doi.org/10.1016/j.palaeo.2023.111450>, 2023.
- 941 Head, M. J. and Gibbard, P. L.: Early–Middle Pleistocene transitions: Linking terrestrial and
942 marine realms, *Quaternary International*, 389, 7-46,
943 <https://doi.org/10.1016/j.quaint.2015.09.042>, 2015.



- 944 Hernández-Almeida, I., Sierro, F. J., Cacho, I., and Flores, J. A.: Subsurface North Atlantic
945 warming as a trigger of rapid cooling events: evidence from the early Pleistocene (MIS 31–
946 19), *Clim. Past*, 11, 687-696, <https://doi.org/10.5194/cp-11-687-2015>, 2015.
- 947 Hernández-Almeida, I., Sierro, F. J., Flores, J.-A., Cacho, I., and Filippelli, G. M.:
948 Palaeoceanographic changes in the North Atlantic during the Mid-Pleistocene Transition
949 (MIS 31–19) as inferred from planktonic foraminiferal and calcium carbonate records,
950 *Boreas*, 42, 140-159, <https://doi.org/10.1111/j.1502-3885.2012.00283.x>, 2013.
- 951 Hernández-Molina, F. J., Sierro, F. J., Llave, E., Roque, C., Stow, D. A. V., Williams, T., Lofi,
952 J., Van der Schee, M., Arnáiz, A., Ledesma, S., Rosales, C., Rodríguez-Tovar, F. J., Pardo-
953 Igúzquiza, E., and Brackenridge, R. E.: Evolution of the gulf of Cadiz margin and southwest
954 Portugal contourite depositional system: Tectonic, sedimentary and paleoceanographic
955 implications from IODP expedition 339, *Marine Geology*, 377, 7-39,
956 <http://dx.doi.org/10.1016/j.margeo.2015.09.013>, 2016a.
- 957 Hernández-Molina, F. J., Wählin, A., Bruno, M., Ercilla, G., Llave, E., Serra, N., Rosón, G.,
958 Puig, P., Rebesco, M., Van Rooij, D., Roque, D., González-Pola, C., Sánchez, F., Gómez,
959 M., Preu, B., Schwenk, T., Hanebuth, T. J. J., Sánchez Leal, R. F., García-Lafuente, J.,
960 Brackenridge, R. E., Juan, C., Stow, D. A. V., and Sánchez-González, J. M.: Oceanographic
961 processes and morphosedimentary products along the Iberian margins: A new
962 multidisciplinary approach, *Marine Geology*, 378, 127-156,
963 <https://doi.org/10.1016/j.margeo.2015.12.008>, 2016b.
- 964 Hodell, D., Lourens, L., Crowhurst, S., Konijnendijk, T., Tjallingii, R., Jiménez-Espejo, F.,
965 Skinner, L., Tzedakis, P. C., Abrantes, F., Acton, G. D., Alvarez Zarikian, C. A., Bahr, A.,
966 Balestra, B., Barranco, E. L., Carrara, G., Ducassou, E., Flood, R. D., Flores, J.-A., Furota,
967 S., Grimalt, J., Grunert, P., Hernández-Molina, J., Kim, J. K., Krissek, L. A., Kuroda, J., Li,
968 B., Lofi, J., Margari, V., Martrat, B., Miller, M. D., Nanayama, F., Nishida, N., Richter, C.,
969 Rodrigues, T., Rodríguez-Tovar, F. J., Roque, A. C. F., Sanchez Goñi, M. F., Sierro
970 Sánchez, F. J., Singh, A. D., Sloss, C. R., Stow, D. A. V., Takashimizu, Y., Tzanova, A.,
971 Voelker, A., Xuan, C., and Williams, T.: A reference time scale for Site U1385 (Shackleton
972 Site) on the SW Iberian Margin, *Global and Planetary Change*, 133, 49-64,
973 <https://doi.org/10.1016/j.gloplacha.2015.07.002>, 2015.
- 974 Hodell, D. A. and Channell, J. E. T.: Mode transitions in Northern Hemisphere glaciation: co-
975 evolution of millennial and orbital variability in Quaternary climate, *Clim. Past*, 12, 1805-
976 1828, <https://doi.org/10.5194/cp-12-1805-2016>, 2016.
- 977 Hodell, D. A., Crowhurst, S. J., Lourens, L., Margari, V., Nicolson, J., Rolfe, J. E., Skinner, L.
978 C., Thomas, N. C., Tzedakis, P. C., Mleneck-Vautravers, M. J., and Wolff, E. W.: A 1.5-
979 million-year record of orbital and millennial climate variability in the North Atlantic, *Clim.*
980 *Past*, 19, 607-636, <https://doi.org/10.5194/cp-19-607-2023>, 2023a.
- 981 Hodell, D. A., Crowhurst, S. J., Lourens, L. J., Margari, V., Nicolson, J., Rolfe, J. E., Skinner,
982 L. C., Thomas, N. C., Tzedakis, P. C., Mleneck-Vautravers, M. J., and Wolff, E. W.: Oxygen
983 and carbon isotope data for the planktonic foraminifera *Globigerina bulloides* at IODP Site
984 339-U1385, PANGAEA [dataset], <https://doi.org/10.1594/PANGAEA.951386>, 2023b.
- 985 Huber, R., Meggers, H., Baumann, K.-H., Raymo, M. E., and Henrich, R.: Shell size variation
986 of the planktonic foraminifer *Neogloboquadrina pachyderma* sin. in the Norwegian-
987 Greenland Sea during the last 1.3 Myrs: implications for paleoceanographic reconstructions,
988 *Palaeogeography, Palaeoclimatology, Palaeoecology*, 160, 193-212,
989 [https://doi.org/10.1016/S0031-0182\(00\)00066-3](https://doi.org/10.1016/S0031-0182(00)00066-3), 2000.
- 990 Jansen, E., Fronval, T., Rack, F., and Channell, J. E. T.: Pliocene-Pleistocene ice rafting history
991 and cyclicity in the Nordic Seas during the last 3.5 Myr, *Paleoceanography*, 15, 709-721,
992 2000.



- 993 Johannessen, T., Jansen, E., Flatøy, A., and Ravelo, A. C.: The relationship between surface
994 water masses, oceanographic fronts and paleoclimatic proxies in surface sediments of the
995 Greenland, Iceland, Norwegian Seas, in: Carbon cycling in the glacial ocean: Constraints
996 on the ocean's role in global change, edited by: Zahn, R., Pedersen, T. F., Kaminski, M. A.,
997 and Labeyrie, L., Springer Verlag, Berlin, 61-85, 1994.
- 998 Jonkers, L. and Kučera, M.: Sensitivity to species selection indicates the effect of nuisance
999 variables on marine microfossil transfer functions, *Clim. Past*, 15, 881-891,
1000 <https://doi.org/10.5194/cp-15-881-2019>, 2019.
- 1001 Kaiser, E. A., Caldwell, A., and Billups, K.: North Atlantic Upper-Ocean Hydrography During
1002 the Mid-Pleistocene Transition Evidenced by *Globorotalia truncatulinoides* Coiling Ratios,
1003 *Paleoceanography and Paleoclimatology*, 34, 658-671,
1004 <https://doi.org/10.1029/2018PA003502>, 2019.
- 1005 Kim, J., Goldstein, S. L., Pena, L. D., Jaume-Seguí, M., Knudson, K. P., Yehudai, M., and
1006 Bolge, L.: North Atlantic Deep Water during Pleistocene interglacials and glacials,
1007 *Quaternary Science Reviews*, 269, 107146,
1008 <https://doi.org/10.1016/j.quascirev.2021.107146>, 2021.
- 1009 Kroopnick, P. M.: The distribution of ^{13}C of ΣCO_2 in the world oceans, *Deep Sea Research*
1010 *Part A. Oceanographic Research Papers*, 32, 57-84, 1985.
- 1011 Kučera, M.: Planktonic Foraminifera as Tracers of Past Oceanic Environments, in: Proxies in
1012 Late Cenozoic Paleoceanography, *Developments in Marine Geology*, edited by: Hillaire-
1013 Marcel, C., and de Vernal, A., 1, Elsevier, 213-262, [http://dx.doi.org/10.1016/S1572-5480\(07\)01011-1](http://dx.doi.org/10.1016/S1572-5480(07)01011-1), 2007.
- 1015 Kučera, M., Weinelt, M., Kiefer, T., Pflaumann, U., Hayes, A., Weinelt, M., Chen, M.-T., Mix,
1016 A. C., Barrows, T. T., Cortijo, E., Duprat, J., Juggins, S., and Waelbroeck, C.:
1017 Reconstruction of sea-surface temperatures from assemblages of planktonic foraminifera:
1018 multi-technique approach based on geographically constrained calibration data sets and its
1019 application to glacial Atlantic and Pacific Oceans, *Quaternary Science Reviews*, 24, 951-
1020 998, <https://doi.org/10.1016/j.quascirev.2004.07.014>, 2005.
- 1021 Lisiecki, L. E. and Raymo, M.: A Pliocene-Pleistocene stack of 57 globally distributed benthic
1022 $\delta^{18}\text{O}$ records, *Paleoceanography*, 20, <https://doi.org/10.1029/2004PA001071>, 2005.
- 1023 MARGO Project Members: Constraints on the magnitude and patterns of ocean cooling at the
1024 Last Glacial Maximum, *Nature Geosci*, 2, 127-132, [10.1038/ngeo411](https://doi.org/10.1038/ngeo411), 2009.
- 1025 Marino, M., Maiorano, P., and Flower, B. P.: Calcareous nannofossil changes during the Mid-
1026 Pleistocene Revolution: Paleoecologic and paleoceanographic evidence from North Atlantic
1027 Site 980/981, *Palaeogeography, Palaeoclimatology, Palaeoecology*, 306, 58-69,
1028 <https://doi.org/10.1016/j.palaeo.2011.03.028>, 2011.
- 1029 Marino, M., Maiorano, P., and Lirer, F.: Changes in calcareous nannofossil assemblages during
1030 the Mid-Pleistocene Revolution, *Marine Micropaleontology*, 69, 70-90, 2008.
- 1031 Martin-Garcia, G. M., Alonso-Garcia, M., Sierro, F. J., Hodell, D. A., and Flores, J. A.: Severe
1032 cooling episodes at the onset of deglaciations on the Southwestern Iberian margin from MIS
1033 21 to 13 (IODP site U1385), *Global and Planetary Change*, 135, 159-169,
1034 <http://dx.doi.org/10.1016/j.gloplacha.2015.11.001>, 2015.
- 1035 McClymont, E. L., Sosdian, S. M., Rosell-Melé, A., and Rosenthal, Y.: Pleistocene sea-surface
1036 temperature evolution: Early cooling, delayed glacial intensification, and implications for
1037 the mid-Pleistocene climate transition, *Earth-Science Reviews*, 123, 173-193,
1038 <https://doi.org/10.1016/j.earscirev.2013.04.006>, 2013.
- 1039 Morard, R., Darling, K. F., Weiner, A. K. M., Hassenrück, C., Vanni, C., Cordier, T., Henry,
1040 N., Greco, M., Vollmar, N. M., Milivojevic, T., Rahman, S. N., Siccha, M., Meilland, J.,
1041 Jonkers, L., Quillévéré, F., Escarguel, G., Douady, C. J., de Garidel-Thoron, T., de Vargas,
1042 C., and Kucera, M.: The global genetic diversity of planktonic foraminifera reveals the



- 1043 structure of cryptic speciation in plankton, *Biological Reviews*,
1044 <https://doi.org/10.1111/brv.13065>, 2024.
- 1045 Müller, P. J., Kirst, G., Ruhland, G., von Storch, I., and Rosell-Melé, A.: Calibration of the
1046 alkenone paleotemperature index Uk'37 based on core-tops from the eastern South Atlantic
1047 and the global ocean (60°N-60°S), *Geochim. Cosmochim. Acta*, 62, 1757-1772,
1048 [https://doi.org/10.1016/S0016-7037\(98\)00097-0](https://doi.org/10.1016/S0016-7037(98)00097-0), 1998.
- 1049 Naafs, B. D. A., Hefter, J., and Stein, R.: Millennial-scale ice rafting events and Hudson Strait
1050 Heinrich(-like) Events during the late Pliocene and Pleistocene: a review, *Quaternary
1051 Science Reviews*, 80, 1-28, <http://dx.doi.org/10.1016/j.quascirev.2013.08.014>, 2013.
- 1052 Osman, M. B., Tierney, J. E., Zhu, J., Tardif, R., Hakim, G. J., King, J., and Poulsen, C. J.:
1053 Globally resolved surface temperatures since the Last Glacial Maximum, *Nature*, 599, 239-
1054 244, <https://doi.org/10.1038/s41586-021-03984-4>, 2021.
- 1055 Peliz, A., Dubert, J., Santos, A. M. P., Oliveira, P. B., and Le Cann, B.: Winter upper ocean
1056 circulation in the Western Iberian Basin—Fronts, Eddies and Poleward Flows: an overview,
1057 *Deep Sea Research Part I: Oceanographic Research Papers*, 52, 621-646,
1058 <https://doi.org/10.1016/j.dsr.2004.11.005>, 2005.
- 1059 Peliz, A., Marchesiello, P., Santos, A. M. P., Dubert, J., Teles-Machado, A., Marta-Almeida,
1060 M., and Le Cann, B.: Surface circulation in the Gulf of Cadiz: 2. Inflow-outflow coupling
1061 and the Gulf of Cadiz slope current, *Journal of Geophysical Research*, 114,
1062 <https://doi.org/10.1029/2008jc004771>, 2009.
- 1063 Pena, L. D. and Goldstein, S. L.: Thermohaline circulation crisis and impacts during the mid-
1064 Pleistocene transition, *Science*, 345, 318-322, <https://doi.org/10.1126/science.1249770>,
1065 2014.
- 1066 Pflaumann, U., Duprat, J., Pujol, C., and Labeyrie, L. D.: SIMMAX: A modern analog
1067 technique to deduce Atlantic sea surface temperatures from planktonic foraminifera in deep-
1068 sea sediments, *Paleoceanography*, 11, 15-36, 1996.
- 1069 Pflaumann, U., Sarnthein, M., Chapman, M., de Abreu, L., Funnell, B., Huels, M., Kiefer, T.,
1070 Maslin, M., Schulz, H., Swallow, J., van Kreveland, S., Vautravers, M., Vogelsang, E., and
1071 Weinelt, M.: Glacial North Atlantic: Sea-surface conditions reconstructed by GLAMAP
1072 2000, *Paleoceanography*, 18, <https://doi.org/10.1029/2002PA000774> 2003.
- 1073 Railsback, L. B., Gibbard, P. L., Head, M. J., Voarintsoa, N. R. G., and Toucanne, S.: An
1074 optimized scheme of lettered marine isotope substages for the last 1.0 million years, and the
1075 climatostratigraphic nature of isotope stages and substages, *Quaternary Science Reviews*,
1076 111, 94-106, <http://dx.doi.org/10.1016/j.quascirev.2015.01.012>, 2015.
- 1077 Raymo, M. E., Ruddiman, W. F., Shackleton, N. J., and Oppo, D. W.: Evolution of Atlantic-
1078 Pacific $\delta^{13}C$ gradients over the last 2.5 m.y., *Earth and Planetary Science Letters*, 97, 353-
1079 368, 1990.
- 1080 Raymo, M. E., Oppo, D. W., Flower, B. P., Hodell, D. A., McManus, J. F., Venz, K. A.,
1081 Kleiven, K. F., and McIntyre, K.: Stability of North Atlantic water masses in face of
1082 pronounced climate variability during the Pleistocene, *Paleoceanography*, 19,
1083 <https://doi.org/10.1029/2003PA000921>, 2004.
- 1084 Reagan, J. R., Boyer, T. P., García, H. E., Locarnini, R. A., Baranova, O. K., Bouchard, C.,
1085 Cross, S. L., Mishonov, A. V., Paver, C. R., Seidov, D., Wang, Z., and Dukhovskoy, D.:
1086 World Ocean Atlas 2023, NCEI Accession 0270533, NOAA National Centers for
1087 Environmental Information [dataset], 2024.
- 1088 Relvas, P., Barton, E. D., Dubert, J., Oliveira, P. B., Peliz, A., da Silva, J. C. B., and Santos, A.
1089 M. P.: Physical oceanography of the western Iberia ecosystem: Latest views and challenges,
1090 *Progress in Oceanography*, 74, 149-173, [10.1016/j.pocean.2007.04.021](https://doi.org/10.1016/j.pocean.2007.04.021), 2007.
- 1091 Rodrigues, T., Voelker, A. H. L., Grimalt, J. O., Abrantes, F., and Naughton, F.: Iberian Margin
1092 sea surface temperature during MIS 15 to 9 (580-300 ka): Glacial suborbital variability



- 1093 versus interglacial stability, *Paleoceanography*, 26, <https://doi.org/10.1029/2010PA001927>,
1094 2011.
- 1095 Rodrigues, T., Alonso-García, M., Hodell, D. A., Rufino, M., Naughton, F., Grimalt, J. O.,
1096 Voelker, A. H. L., and Abrantes, F.: A 1-Ma record of sea surface temperature and extreme
1097 cooling events in the North Atlantic: A perspective from the Iberian Margin, *Quaternary*
1098 *Science Reviews*, 172, 118-130, <https://doi.org/10.1016/j.quascirev.2017.07.004>, 2017.
- 1099 Rodrigues, T., Alonso-García, M., Hodell, D. A., Rufino, M. M., Naughton, F., Grimalt, J. O.,
1100 Voelker, A. H. L., and Abrantes, F. F.: A 1 Ma record of Sea Surface Temperature and
1101 extreme cooling events in the North Atlantic: A perspective from the Iberian Margin,
1102 PANGAEA [dataset], <https://doi.org/10.1594/PANGAEA.921577>, 2020.
- 1103 Rufino, M. M., Salgueiro, E., Voelker, A. A. H. L., Polito, P. S., Cermeño, P. A., and Abrantes,
1104 F.: Ocean kinetic energy and photosynthetic biomass are important drivers of planktonic
1105 foraminifera diversity in the Atlantic Ocean, *Frontiers in Marine Science*, 9,
1106 <https://doi.org/10.3389/fmars.2022.887346>, 2022.
- 1107 Salgueiro, E., Voelker, A. H. L., de Abreu, L., Abrantes, F., Meggers, H., and Wefer, G.:
1108 Temperature and productivity changes off the western Iberian margin during the last 150
1109 ky, *Quaternary Science Reviews*, 29, 680-695,
1110 <https://doi.org/10.1016/j.quascirev.2009.11.013>, 2010.
- 1111 Salgueiro, E., Naughton, F., Voelker, A. H. L., de Abreu, L., Alberto, A., Rossignol, L., Duprat,
1112 J., Magalhães, V. H., Vaqueiro, S., Turon, J. L., and Abrantes, F.: Past circulation along the
1113 western Iberian margin: a time slice vision from the Last Glacial to the Holocene,
1114 *Quaternary Science Reviews*, 106, 316-329,
1115 <https://doi.org/10.1016/j.quascirev.2014.09.001>, 2014.
- 1116 Salgueiro, E., Voelker, A., Abrantes, F., Meggers, H., Pflaumann, U., Loncaric, N., Gonzalez-
1117 Alvarez, R., Oliveira, P., Bartels-Jonsdottir, H. B., Moreno, J., and Wefer, G.: Planktonic
1118 foraminifera from modern sediments reflect upwelling patterns off Iberia: Insights from a
1119 regional transfer function, *Marine Micropaleontology*, 66, 135-164,
1120 <https://doi.org/10.1016/j.marmicro.2007.09.003>, 2008.
- 1121 Sanchez, R. F. and Relvas, P.: Spring-summer climatological circulation in the upper layer in
1122 the region of Cape St. Vincent, Southwest Portugal, *ICES Journal of Marine Science*, 60,
1123 1232-1250, [https://doi.org/10.1016/S1054-3139\(03\)00137-1](https://doi.org/10.1016/S1054-3139(03)00137-1), 2003.
- 1124 Sarthein, M., Winn, K., Jung, S., Duplessy, J., Labeyrie, L., Erlenkeuser, H., and Ganssen,
1125 G.: Changes in east Atlantic deepwater circulation over the last 30,000 years: Eight time
1126 slices reconstructions, *Paleoceanography*, 9, 209-267, 1994.
- 1127 Schiebel, R. and Hemleben, C.: *Planktic Foraminifers in the Modern Ocean*, Springer Verlag,
1128 Berlin Heidelberg, 358 pp., <https://doi.org/10.1007/978-3-662-50297-6>, 2017.
- 1129 Schlitzer, R.: Ocean Data View, odv.awi.de [code], 2023.
- 1130 Serrano, F. and Guerra-Merchán, A.: Sea-surface temperature for left-coiling
1131 *Neogloboquadrina* populations inhabiting the westernmost Mediterranean in the middle
1132 Pleistocene and the Pleistocene-Pliocene transition, *Geobios*, 45, 231-240,
1133 <https://doi.org/10.1016/j.geobios.2011.04.003>, 2012.
- 1134 Shackleton, N. J.: The 100,000-Year Ice-Age Cycle Identified and Found to Lag Temperature,
1135 Carbon Dioxide, and Orbital Eccentricity, *Science*, 289, 1897-1902, 2000.
- 1136 Shackleton, N. J., Hall, M. A., and Vincent, E.: Phase relationships between millennial-scale
1137 events 64,000-24,000 years ago, *Paleoceanography*, 15, 565-569, 2000.
- 1138 Singh, A. D., Verma, K., Jaiswal, S., Alonso-García, M., Li, B., and Abrantes, F.: Planktic
1139 foraminiferal responses to orbital scale oceanographic changes off the western Iberian
1140 margin over the last 900 kyr: Results from IODP site U1391, *Global and Planetary Change*,
1141 135, 47-56, <http://dx.doi.org/10.1016/j.gloplacha.2015.10.002>, 2015.



- 1142 Singh, H., Singh, A. D., Tripathi, R., Singh, P., Verma, K., Voelker, A. H. L., and Hodell, D.
1143 A.: Centennial-millennial scale ocean-climate variability in the northeastern Atlantic across
1144 the last three terminations, *Global and Planetary Change*, 223, 104100,
1145 <https://doi.org/10.1016/j.gloplacha.2023.104100>, 2023.
- 1146 Stein, R., Hefter, J., Gruetzner, J., Voelker, A., and Naafs, B. D. A.: Variability of surface-
1147 water characteristics and Heinrich-like Events in the Pleistocene mid-latitude North Atlantic
1148 Ocean: Biomarker and XRD records from IODP Site U1313 (MIS 16 – 9),
1149 *Paleoceanography*, 24, <https://doi.org/10.1029/2008PA001639>, 2009.
- 1150 Storz, D., Schulz, H., Waniek, J. J., Schulz-Bull, D. E., and Kucera, M.: Seasonal and
1151 interannual variability of the planktic foraminiferal flux in the vicinity of the Azores
1152 Current, *Deep Sea Research Part I: Oceanographic Research Papers*, 56, 107-124, 2009.
- 1153 Sun, Y., McManus, J. F., Clemens, S. C., Zhang, X., Vogel, H., Hodell, D. A., Guo, F., Wang,
1154 T., Liu, X., and An, Z.: Persistent orbital influence on millennial climate variability through
1155 the Pleistocene, *Nat Geosci*, 14, 812-818, <https://doi.org/10.1038/s41561-021-00794-1>,
1156 2021.
- 1157 Tachikawa, K., Rapuc, W., Vidal, L., Dubois-Dauphin, Q., Westerhold, T., Guihou, A.,
1158 Bickert, T., Pérez-Asensio, J. N., Deschamps, P., and Skonieczny, C.: Eastern Atlantic deep-
1159 water circulation and carbon storage inferred from neodymium and carbon isotopic
1160 compositions over the past 1.1 million years, *Quaternary Science Reviews*, 252, 106752,
1161 <https://doi.org/10.1016/j.quascirev.2020.106752>, 2021.
- 1162 Tierney, J. E., Zhu, J., King, J., Malevich, S. B., Hakim, G. J., and Poulsen, C. J.: Glacial
1163 cooling and climate sensitivity revisited, *Nature*, 584, 569-573,
1164 <https://doi.org/10.1038/s41586-020-2617-x>, 2020.
- 1165 Ujiie, Y., de Garidel-Thoron, T., Watanabe, S., Wiebe, P., and de Vargas, C.: Coiling
1166 dimorphism within a genetic type of the planktonic foraminifer *Globorotalia*
1167 *truncatulinoides*, *Marine Micropaleontology*, 77, 145-153,
1168 <http://dx.doi.org/10.1016/j.marmicro.2010.09.001>, 2010.
- 1169 Vargas, J. M., Garcia-Lafuente, J., Delgado, J., and Criado, F.: Seasonal and wind-induced
1170 variability of Sea Surface Temperature patterns in the Gulf of Cadiz, *Journal of Marine*
1171 *Systems*, 38, 205-219, 2003.
- 1172 Ventura, C., Abrantes, F., Loureiro, I., and Voelker, A. H. L.: Data report: diatom and
1173 silicoflagellate records of marine isotope Stages 25–27 at IODP Site U1387, Faro Drift,
1174 <https://doi.org/10.2204/iodp.proc.339.202.2017>, 2017.
- 1175 Villanueva, J., Grimalt, J. O., Cortijo, E., Vidal, L., and Labeyrie, L.: A biomarker approach to
1176 the organic matter deposited in the North Atlantic during the last climatic cycle, *Geochim.*
1177 *Cosmochim. Acta*, 61, 4633-4646, 1997.
- 1178 Voelker, A. H. L. and de Abreu, L.: A Review of Abrupt Climate Change Events in the
1179 Northeastern Atlantic Ocean (Iberian Margin): Latitudinal, Longitudinal and Vertical
1180 Gradients, in: *Abrupt Climate Change: Mechanisms, Patterns, and Impacts*, edited by:
1181 Rashid, H., Polyak, L., and Mosley-Thompson, E., *Geophysical Monograph Series*, 193,
1182 AGU, Washington D.C., 15-37, <https://doi.org/10.1029/2010GM001021>, 2011.
- 1183 Voelker, A. H. L. and Salgueiro, E.: Planktonic foraminifera assemblages in NE Atlantic and
1184 Alboran Sea surface sediments, *PANGAEA* [dataset],
1185 <https://doi.org/10.1594/PANGAEA.878069>, 2017.
- 1186 Voelker, A. H. L., de Abreu, L., Schönfeld, J., Erlenkeuser, H., and Abrantes, F.: Hydrographic
1187 Conditions Along the Western Iberian Margin During Marine Isotope Stage 2, *Geochem.*
1188 *Geophys. Geosyst.*, 10, <https://doi.org/10.1029/2009GC002605>, 2009.
- 1189 Voelker, A. H. L., Rodrigues, T., Trotta, S., Marino, M., and Kuhnert, H.: A Southern
1190 Portuguese Margin Perspective of Marine Isotope Stage 47 – An Interglacial in the 41 kyr
1191 World, *Atmosphere*, 13, 1-25, <https://doi.org/10.3390/atmos13091378>, 2022.



- 1192 Voelker, A. H. L., Jimenez-Espejo, F. J., Bahr, A., Rebotim, A., Cavaleiro, C., Salgueiro, E.,
1193 and Röhl, U.: Data report: IODP Site U1387: the revised splice between Sections U1387B-
1194 18X-3 and U1387C-8R-3 (>171.6 mcd), <https://doi.org/10.2204/iodp.proc.339.204.2018>,
1195 2018.
- 1196 Voelker, A. H. L., Salgueiro, E., Rodrigues, T., Jimenez-Espejo, F. J., Bahr, A., Alberto, A.,
1197 Loureiro, I., Padilha, M., Rebotim, A., and Röhl, U.: Mediterranean Outflow and surface
1198 water variability off southern Portugal during the early Pleistocene: A snapshot at Marine
1199 Isotope Stages 29 to 34 (1020–1135 ka), *Global and Planetary Change*, 133, 223–237,
1200 <https://doi.org/10.1016/j.gloplacha.2015.08.015>, 2015.
- 1201 Westerhold, T., Marwan, N., Drury, A. J., Liebrand, D., Agnini, C., Anagnostou, E., Barnet, J.
1202 S. K., Bohaty, S. M., De Vleeschouwer, D., Florindo, F., Frederichs, T., Hodell, D. A.,
1203 Holbourn, A. E., Kroon, D., Laurentino, V., Littler, K., Lourens, L. J., Lyle, M., Pälike, H.,
1204 Röhl, U., Tian, J., Wilkens, R. H., Wilson, P. A., and Zachos, J. C.: An astronomically dated
1205 record of Earth’s climate and its predictability over the last 66 million years, *Science*, 369,
1206 1383–1387, <https://doi.org/10.1126/science.aba6853>, 2020.
- 1207 Willeit, M., Ganopolski, A., Calov, R., and Brovkin, V.: Mid-Pleistocene transition in glacial
1208 cycles explained by declining CO₂ and regolith removal, *Science Advances*, 5, eaav7337,
1209 <https://doi.org/10.1126/sciadv.aav7337>, 2019.
- 1210 Wright, A. K. and Flower, B. P.: Surface and deep ocean circulation in the subpolar North
1211 Atlantic during the mid-Pleistocene revolution, *Paleoceanography*, 17,
1212 <https://doi.org/10.1029/2002PA000782>, 2002.
- 1213
1214